UNIVERSIDAD DE INVESTIGACIÓN DE TECNOLOGÍA EXPERIMENTAL YACHAY

Escuela de Ciencias Físicas y Nanotecnología

TÍTULO: Fabrication of PVP Nanofibers with Carbon Nanotubes and Cobalt Ferrite Nanoparticles

Trabajo de integración curricular presentado como requisito para la obtención del título de Ingeniero en Nanotecnología

Autor:

Cevallos Durán Vinicio Javier

Tutora:

Ph.D. - Briceño Araujo Sarah Elisa

Co-tutor:

Ph.D. - Dávalos Raúl

Urcuquí, Marzo del 2024

Autoría

Yo, **Vinicio Javier Cevallos Durán**, con cédula de identidad 0106983026, declaro que las ideas, juicios, valoraciones, interpretaciones, consultas bibliográficas, definiciones y conceptualizaciones expuestas en el presente trabajo; así cómo, los procedimientos y herramientas utilizadas en la investigación, son de absoluta responsabilidad de el autor del trabajo de integración curricular. Así mismo, me acojo a los reglamentos internos de la Universidad de Investigación de Tecnología Experimental Yachay.

Urcuquí, Marzo del 2024.

Vinicio Javier Cevallos Durán
CI:0106983026

Autorización de publicación

Yo, **Vinicio Javier Cevallos Durán**, con cédula de identidad 0106983026, cedo a la Universidad de Investigación de Tecnología Experimental Yachay, los derechos de publicación de la presente obra, sin que deba haber un reconocimiento económico por este concepto. Declaro además que el texto del presente trabajo de titulación no podrá ser cedido a ninguna empresa editorial para su publicación u otros fines, sin contar previamente con la autorización escrita de la Universidad.

Asimismo, autorizo a la Universidad que realice la digitalización y publicación de este trabajo de integración curricular en el repositorio virtual, de conformidad a lo dispuesto en el Art. 144 de la Ley Orgánica de Educación

Urcuquí, Marzo del 2024.

<div align="center">

Vinicio Javier Cevallos Durán
CI: 0106983026

</div>

Dedication

To Ruth and Manuel

This work expresses the final part of my career. However, I could only have achieved it with your support and belief in me over these years.

Vinicio Javier Cevallos Durán

Acknowledgments

Resumen

La fabricación de nanofibras de polivinilpirrolidona (PVP) incrustadas con nanotubos de carbono de pared múltiple (MWCNTs) y nanopartículas de ferrita de cobalto (CoFe2O4) (5, 10, 15, 20 y 25 nm) se logró a través del proceso de electrohilado, obteniendo diámetros promedio de a) PVP 4.13 μm, b) PVP/CoFe2O4 (5 nm) 2.23 μm, c) PVP/CoFe2O4 (10 nm) 1.20 μm, d) PVP/CoFe2O4 (15 nm) 1.83 μm, e) PVP/CoFe2O4 (20 nm) 2.29 μm, f) PVP/CoFe2O4 (25 nm) 1.95 μm, g) PVP/MWCNTs 2.12 μm, h) PVP/MWCNTs/CoFe2O4 (5 nm) 0.55 μm, i) PVP/MWCNTs/CoFe2O4 (10 nm) 0.68 μm, j) PVP/MWCNTs/CoFe2O4 (15 nm) 1.07 μm, k) PVP/MWCNTs/CoFe2O4 (20 nm) 0.55 μm y l) PVP/MWCNTs/CoFe2O4 (25 nm) 1.06 μm. Se realizó un estudio para caracterizar las propiedades estructurales utilizando microscopía óptica, espectroscopía Raman, espectroscopía infrarroja por transformada de Fourier (FTIR) y análisis termogravimétrico (TGA). Los resultados muestran la formación de fibras con nanotubos de carbono de pared múltiple y nanopartículas de ferrita de cobalto. Además, la técnica de voltaje vs resistencia muestra un aumento de las propiedades eléctricas de las fibras compuestas en relación con las fibras de polímero. Se logra un aumento de 0.08 V a 4.20 V con un voltaje aplicado de 421 V. Disminuye la resistencia de 52GΩ a 0.99GΩ, respectivamente. La combinación de polivinilpirrolidona con nanopartículas de ferrita de cobalto y nanotubos de carbono proporciona versatilidad en la adaptación de las propiedades de las nanofibras. Este trabajo estudia la optimización de las fibras contra el tamaño de las nanopartículas de cobalto para optimizar las propiedades estructurales, magnéticas y eléctricas como materiales potenciales para biosensores.

Palabras clave: Nanofibras, electrohilado, nanopartículas de hierro-cobalto, nanotubos de carbono.

Abstract

The fabrication of polyvinylpyrrolidone (PVP) nanofibers embedded with multi-walled carbon nanotubes (MWCNTs) and cobalt ferrite ($CoFe_2O_4$) nanoparticles (5, 10, 15, 20, and 25 nm) was achieved through the electrospinning process, obtaining average diameters of a) PVP 4.13 μm, b) PVP/$CoFe_2O_4$ (5nm) 2.23 μm, c) PVP/$CoFe_2O_4$ (10nm) 1.20 μm, d) PVP/$CoFe_2O_4$ (15nm) 1.83 μm, e) PVP/$CoFe_2O_4$ (20nm) 2.29 μm, f) PVP/$CoFe_2O_4$ (25nm) 1.95 μm, g) PVP/MWCNTs 2.12 μm, h) PVP/MWCNTs/$CoFe_2O_4$ (5nm) 0.55 μm, i) PVP/MWCNTs/$CoFe_2O_4$ (10nm) 0.68 μm, j) PVP/MWCNTs/$CoFe_2O_4$ (15nm) 1.07 μm, k) PVP/MWCNTs/$CoFe_2O_4$ (20nm) 0.55 μm and l) PVP/MWCNTs/$CoFe_2O_4$ (25nm) 1.06 μm. A study was conducted to characterize the structural properties using Optical microscopy, Raman spectroscopy, Fourier Transform Infrared spectroscopy (FTIR), and Thermogravimetric analysis (TGA). The results show the formation of fibers with multi-walled carbon nanotubes and cobalt ferrite nanoparticles. Furthermore, the voltage vs resistance technique shows an increment of electrical properties of composite fibers concerning polymer fibers. Achieving an increment from 0.08 V to 4.20 V with an applied voltage of 421 V. It decreases resistance from 52GΩ to 0.99GΩ, respectively. The combination of polyvinyl pyrrolidone with cobalt ferrite nanoparticles and carbon nanotubes provides versatility in tailoring the properties of nanofibers. This work studies the optimization of the fibers against the size of cobalt nanoparticles to optimize the structural, magnetic, and electric properties as potential materials for biosensing.

Keywords: Nanofibers, electrospinning, cobalt-ferrite nanoparticles, carbon nanotubes.

Contents

iii

List of Figures

List of Tables

Chapter 1

Introduction

Due to their industrial, scientific, and technological applications, the recent developments in material science and semiconductors, specifically in sensors, make them a fundamental key in our lives. The sensors are devices capable of detecting and measuring physical, mechanical, and chemical changes, giving real-time information and allowing an automatization process[1]. Some types of sensors, such as electrical, chemical, optical, physical, and mechanical, give a multidisciplinary list of applications in many fields, including environmental, biomedical, energy, physical devices, and others[1]. Nevertheless, sensing properties such as electrical conductivity, light, and temperature are some challenges sensors have in the industrial and technology sectors[1].

Nowadays, nanotechnology advancements have significantly impacted sensors due to nanostructured materials providing shorter pathways for electron transfer along the nanofiber's longitudinal axis, improving sensing performance[2]. Several methods can produce nanofibers, such as phase separation, wet spinning, template synthesis, and drawing[3]. However, these methods are not accessible due to high costs and are not sustainable for all polymers[3]. Electrospinning (ES) is one of the most powerful and facile techniques for producing organized and complex uniform fibers and controlling the diameter and morphology of synthetic and natural polymers[4]. Typically, fiber's diameters range from few nanometers to several micrometers[4].

In the last years, researchers have used several materials polymer for electrospinning, such as polyvinyl alcohol (PVA), polyvinylpyrrolidone (PVP), polyaniline, polycarbonate, polyethylene oxide, polystyrene, polyacrylonitrile, etc[5]. Polyvinylpyrrolidone has taken significant attention due to its good biocompatibility, excellent film formation ability, and non-toxic behavior, which make it one of the most important

1

materials used in paints, electronics, and biomedical engineering[6].

Carbon nanotubes (CNTs) show unique electrical, mechanical, and magnetic properties. These properties make CNTs being used for fabricating sensors and biosensors. CNTs have a high surface area and adsorption ability, making them an excellent option for fabricating chemical and biological sensors with high sensitivity and selectivity[7]. Furthermore, magnetic nanoparticles have become increasingly popular due to their magnetic properties and potential applications in various fields. $CoFe_2O_4$ nanoparticles can be synthesized using different methods, such as co-precipitation, thermal decomposition method, sol-gel, coprecipitation method and hydrothermal methods[8], which enable precise control over the particle size, shape, and surface chemistry[9].

In previous studies, Nasouri et al.(2016)[10] developed a composite nanofiber of PVP filled with multi-walled carbon nanotubes (MWCNTs) by electrospinning. The electrical conductivity and complex permittivity of MWCNTs/PVP composite nanofibers increased when the concentration of MWCNTs increased, too. Furthermore, Li et al. (2023)[11] designed a flexible nanofiber membrane with $CoFe_2O_4$ nanoparticles embedded in N-doped carbon nanofibers. They showed that the presence of $CoFe_2O_4$ nanoparticles in the nanofiber membrane helped to improve the electrical conductivity. Additionally, Alghamdi, H. M., & Rajeh, A. (2022) synthesized a $CoFe_2O_4$/MWCNTs nanohybrid to create polymer nanocomposite films based on CMC/PVA. They observed that the energy gap of nanocomposite film decreased from 5.32 to 3.97 eV for the direct transition and 4.89 to 3.58 eV for the indirect transition due to the increment of concentration of $CoFe_2O_4$/MWCNTs in the polymer blend. Therefore, adding nanomaterials as $CoFe_2O_4$ nanoparticles and MWCNTs into a polymer matrix makes a promising composite material to improve the electrical conductivity in sensors.

The aim of this work is to fabricate nanofibers of PVP with carbon nanotubes and nanoparticles of $CoFe_2O_4$ (5, 10, 15, 20, and 25 nm) by electrospinning technique to study the electrical properties of the fiber composites.

1.1 Problem Statement

Research on improving the electrical properties of insulator polymers is crucial to semiconductor devices. The fast growth in the semiconductor industry, projected to become a trillion-dollar by 2030[12], has made many scientists focus on combining semiconductor and material science fields to achieve better results in electrical conductivity. Nowadays, insulator polymers such as PVA, PVP, and PE are used to enhance their electrical properties using nanomaterials. Polyvinylpyrrolidone (PVP) exhibits properties as it is highly soluble in water and organic solvents, has biocompatibility, and can form micro-nanofibers and films, making it a good candidate. For that reason, fabricating micro or nanofibers of PVP loaded with nanomaterials by electrospinning technique is an area that has gained more attention in developed countries due to the reduced response time of sensors.

1.2 General and Specific Objectives

1.2.1 General objective

- To fabricate PVP nanofibers loaded with carbon nanotubes and $CoFe_2O_4$ nanoparticles.

1.2.2 Specific objectives

- To synthesize $CoFe_2O_4$ nanoparticles at different sizes.

- To optimize the relation between PVP, CNTs, and $CoFe_2O_4$ nanoparticles.

- To fabricate composite nanofibers using the electrospinning technique.

- To characterize the nanofibers using Optical Microscopy, Raman spectroscopy, FTIR, and TGA.

- To study the electrical properties of nanofibers using a voltage as a function of resistance characterization.

Chapter 2

Theoretical Background

2.1 Nanotechnology

The concept of nanotechnology is attributed to famous Nobel Laureate Dr. Richard P. Feynman, who called his science lectures as "There's Plenty of Room at the Bottom: An Invitation to Enter a New Field of Physics"[13]. Nanotechnology word comes from the Greek prefix "nano" which refers to a reduction in size or time of 10−9. The nanoscale range is typically defined from 1 to 100 nm in which dramatic alterations may occur in the properties of materials such as physical, chemical, and biological, which may be quite different for a bulk material[14]. Many authors defined nanotechnology as technology on the nanoscale with many applications in the real world. Furthermore, the dictionary definition of nanotechnology is "the design, characterization, manufacture and shape and size-controlled application of matters in the nanoscale" (dictionary definition)[14][15]. Therefore, nanotechnology can play an important role in developing and improving methods used to produce new products, reducing material and energy consumption[14].

2.1.1 Nanoparticles

A nanoparticle is defined as a group of atoms (between 10-10^5) bonded together with an average radius between 1 and 100 nm[14]. The nanoparticles show better performance properties than bulk materials used for similar applications due to the increment of their superficial area. NPs offer a wide range of applications such as sensor, electronic (solar energy conversion), environmental (water treatment), and biological[14]. In general, nanoparticles are used for electronic devices due to high electric conductivity, good oxidation resistance and easiness for large-scale preparation[16].

2.1.2 CoFe$_2$O$_4$ Nanoparticles

Recently, there has been an increment in interest in studying magnetic nanoparticles (MNPs), specifically cobalt ferrite nanoparticles (CoFe$_2$O$_4$). Ferrites can combine physical properties with high chemical stability, and the cost of production is low[17]. In the same way, iron oxides and cobalt are known as highly attractive magnetic materials due to their properties and low-cost production[17]. Nevertheless, Chen (2014) et al. showed that CoFe$_2$O$_4$ sensor materials have better electro-catalytic properties than Fe2O3 and Co3O4 due to the synergy between different elements[18,19], making CoFe$_2$O$_4$ nanoparticles a nanoparticles a promising material for electronic devices.

2.1.3 Carbon nanotubes

Carbon nanotubes were introduced in 1911 by Iijima[20]. CNTs form a graphene cylindrical tube with diameters ranging from one nanometer to several nanometers and show relevant properties such as small size and mass, high electrical, conductivity, and thermal conductivity, making CNTs have numerous applications in thermal, mechanical, electronic, and biological applications[14]. CNTs can be synthesized by chemical vapor deposition (CVD), laser ablation, metal-catalyzed disproportionation, and their combination[14]. The different parameters at the moment of synthesis allow multi-walled carbon nanotubes or single-walled carbon nanotubes (SWCNT) to be obtained.

2.2 Polymer

The word polymers is derived from the Greek words 'poly'= many and 'meros'= part, so a polymer is defined as a large molecule formed by numerous smaller molecules called monomers[21]. The polymer molecule size may be defined as the number of repeat units in the molecule, called the polymerization degree[21]. There is no specific method to classify polymers. One way is to consider the thermal treatment in which polymers are classified into thermoplastics and thermosets. Thermoplastic refers to polymers that melt when heated and resolidify when cooled, and thermosets are polymers that do not melt when heated; however, they decompose irreversibly at high temperatures[21]. Another classification method is based on the nature of the chemical reactions used in polymerization. *Condesation polymers* are formed from monomers in which reaction goes with the loss of a small molecule (usually water), while the *addition polymers* are composed by the addition of reaction of an unsaturated monomer[21].

2.2.1 Polyvinylpyrrolidone

Polyvinylpyrrolidone is a synthetic, non-toxic and non-ionic polymer composed of C=O, C-N and CH$_2$ functional groups (Fig2.1. a and b) in which each PVP molecule contains hydrophilic component (pyrrolidone moiety) and a hydrophobic group (alkyl group)[6,22]. Non-aqueous liquids (such as ethanol) and water are excellent solvents for PVP due to this polymer exhibiting the presence of a strongly polar amide group within the pyrrolidone ring, along with nonpolar methylene and methine groups found both in the ring and along its backbone[22]. Furthermore, considering the hydrophobic carbon chains of the PVP structure, this polymer is a good stabilizer due to the repulsive force that prevents the aggregation of nanoparticles[22].
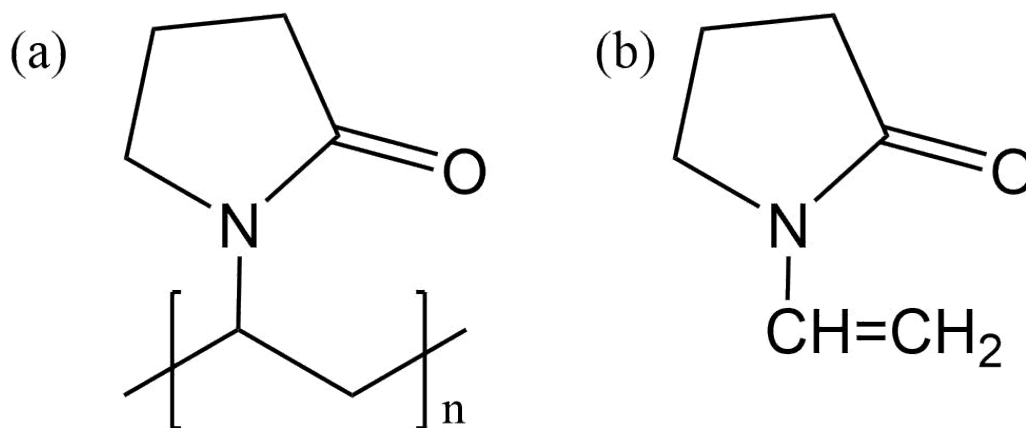
Figure 2.1: (a) Chemical structure of poly (vinyl pyrrolidone)[6] and (b) molecular structure of the monomer N-vinylpyrrolidone[22].

2.3 Electrospinning

The term 'electrospinning' was introduced by Anton Formhals in 1934[23]. Nevertheless, this technique did not get much attention until the 1990s for two reasons. One reason is that the high-voltage electrostatic method was not mature, and the other is that the nanotechnology field was unknown[23]. In 1996, Darell et al. showed that it is a simple and powerful technique to fabricate polymeric fibers with diameters ranging from nanometers to micrometers[23]. The electrospinning equipment consists of a high-voltage power supply, a syringe pump, a metallic needle, and a collector[24], as shown in figure 2.2. First, a polymer solution is loaded into a syringe and driven to a metallic needle by a syringe pump until a droplet is produced at the tip. At this moment, a high voltage is applied to the metallic needle to stretch the droplet, forming the

Taylor cone and then generating an electrified jet. Finally, the jet is elongated and continuously agitated through electrostatic repulsion until it is deposited onto the collector.

There are some parameters to consider when producing fibers, as seen in the figure 2.2.

Control parameters	Effects on fiber morphology
High voltage	(i) The fiber diameter value reduces with the increase in voltage supplied due to the higher stretching of polymer solution [17]. (ii) Higher voltage will increase the evaporation rate that dries the solvent faster [28, 29]. (iii) Lower voltage values result in reduced flight time of the polymer jet, which increases the possibility of obtaining smoother fibers [30].
Concentration	(i) The fiber diameter value increases with a higher concentration of polymer solution. (ii) With lower concentrations, defects in the form of beads start to appear on the nanofiber mat. (iii) Possibility of electrospraying also increases on lower concentrations [8, 12].
Rotational speed	(i) The average fiber diameter value is higher with a stationary rotor than a rotating collector. (ii) The diameter of fibers decreases with an increase in rotating collector RPM, but the decrease in value is not significant compared to other parameters [31].
Collecting distance	(i) Increasing the distance will increase the time of flight, resulting in stretched and further elongated fibers [30]. (ii) Beads start to appear with a higher distance between the needle & the collector. (iii) Formation of beads also takes place with lower distances as the polymer jet does not experience a sufficient time to solidify [32, 33]. (iv) The optimum distance is required to obtain smooth fibers [17].
Flow rate	(i) The fiber diameter decreases with the lower flow rate of polymer solution because it provides more time for stretching [17]. (ii) Higher flow rate values yielded thicker fibers with beads as the drying time for the fibers reduces [33].

Figure 2.2: Effect of electrospinning factors on fiber morphology. Recovered from the reference[24]

2.4 Interdigitated circuits

One of the more important goals in electronics is the ability to comprise two miniaturized interdigitated electrodes (IDE) by MEMS surface micromachining processes so that they are exposed to an aqueous solution containing a target agent[25]. This process is used in sensing applications in the environmental science and biomedical fields. For instance, Tolouei et. al (2020) developed an interdigitated gold-coated sensor for biochemical sensing applications[25] (Fig. 2.3a), and Hu et. al (2020) fabricated an integrated humidity sensor. The sensor comprises a sensitive film of titanium dioxide nanoparticles and interdigitated electrodes[26]. A schematic structure representation is shown in the figure 2.3b.
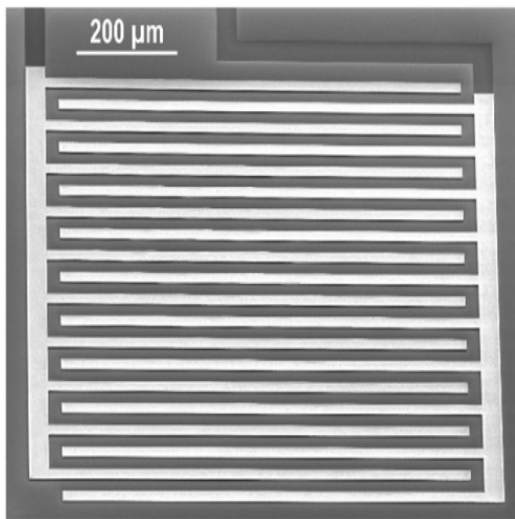
(a) SEM image of the interdigitated gold-coated sensor. Recovered from the reference[25].
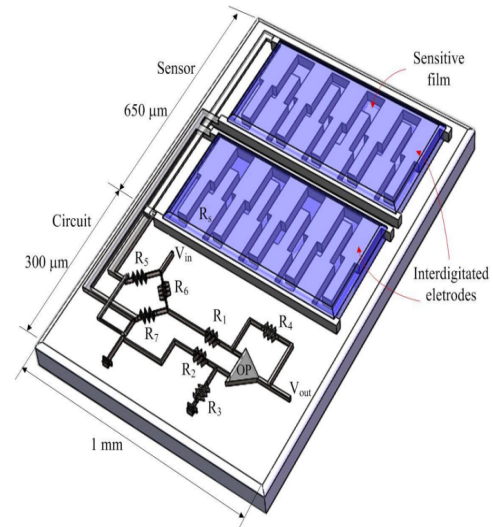
(b) Schematic structure of the integrated humidity sensor. Recovered from the reference[26].

Figure 2.3: Interdigitated circuits developed for sensoring applications.

2.4.1 Mott Transition

The concept of Mott transition explains the electronic phases and physical properties in correlated electron materials by insulator-metal-transition[27]. The nature of the transition depends on the structure of the insulating state[28]. Moreover, understanding the electron dynamics, spin, and lattice across the transition. Mott transition explains the behavior of an electron in a material as a function of the density, which can be

produced by doping as elemental substitution or photoirradiation in transition-metal compounds2–4 and organic materials[27]. Furthermore, Yamakawa et al.[27] (2017) showed the application of a strong electric field can create a Mott transition by a new pathway.

2.5 Characterization techniques

2.5.1 Optical Microscopy

The principle of an optical microscope begins when the light from the microscope lamp goes through the condenser way to the sample, so some of the light passes through the sample and the rest around. It is called direct light[29]. Furthermore, background light passes around the sample, which is also undeviated. The undeviated light is rendered one-half wavelength out of step with the direct light. The one-half wavelength out of phase generates destructive interference with the direct light when they arrive at the intermediate image plane at the eyepiece[29]. The image is magnified by the eye lens of the eyepiece so that this image will projected onto the retina. To obtain high-quality images in microscopy, it is necessary to use proper illumination. For that reason, August Köhler introduced an advanced procedure for microscope illumination in 1893[29]. Most modern laboratory microscopes recommend this technique because the specimen illumination is uniformly bright and free from glare[29].
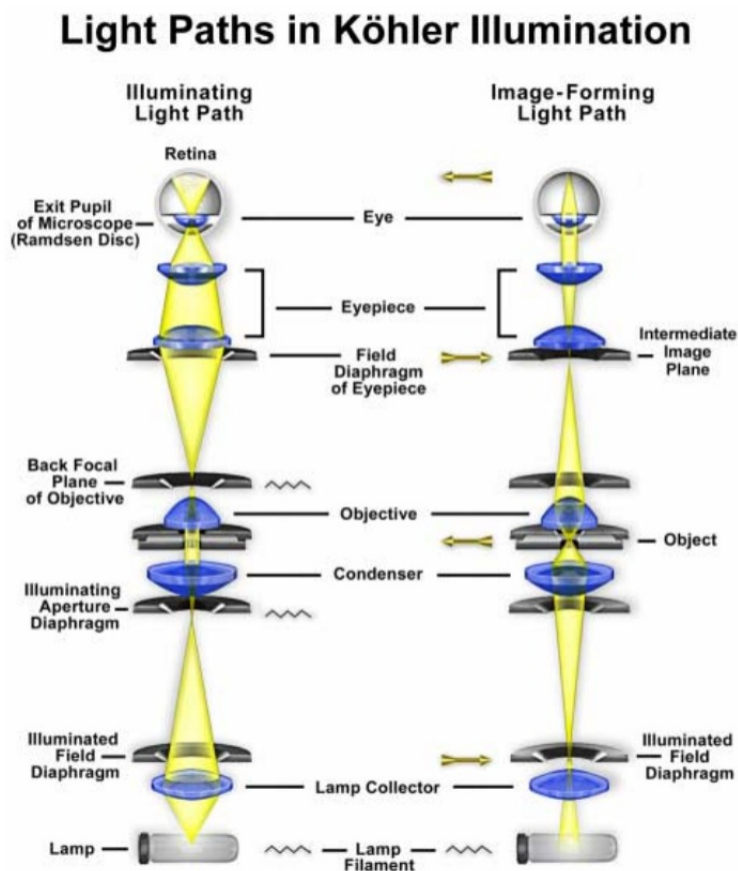
Figure 2.4: Light paths in Kohler illumination. The illuminating ray paths are illustrated on the left side and the image-forming ray paths on the right. Recovered from the reference[29].

2.5.2 Thermogravimetric Analysis (TGA)

Thermogravimetric analysis is used to observe the sample's weight variation with respect to the thermal treatment[30]. It means that some mass will be lost due to sample decomposition, and this weight loss is measured employing a microbalance. Additionally, in the thermogravimetric method, the sample is treated at different temperatures and atmospheres, allowing simultaneous measurement of a sample's temperatures, time, and mass in controlled conditions[30]. The process begins by inserting the sample in a "sample pan" or container. Then, the temperature variation is set according to a customized temperature program, which includes ramp steps at different heating rates[30]. Concerning the PAN, which is usually positioned on a sample holder and connected with the microbalance, the mass variation is measured in

each step as the temperature increases. Furthermore, it is necessary to consider the physical properties of the sample because it can affect the TG curves[30]. Another way of showing the results is called derivative thermogravimetry (DTG). DTG is also used to investigate the kinetic parameters[30]. The TGA signal is reported as T/% of mass, and the DTG is plotted as mg/min or %/min[30].
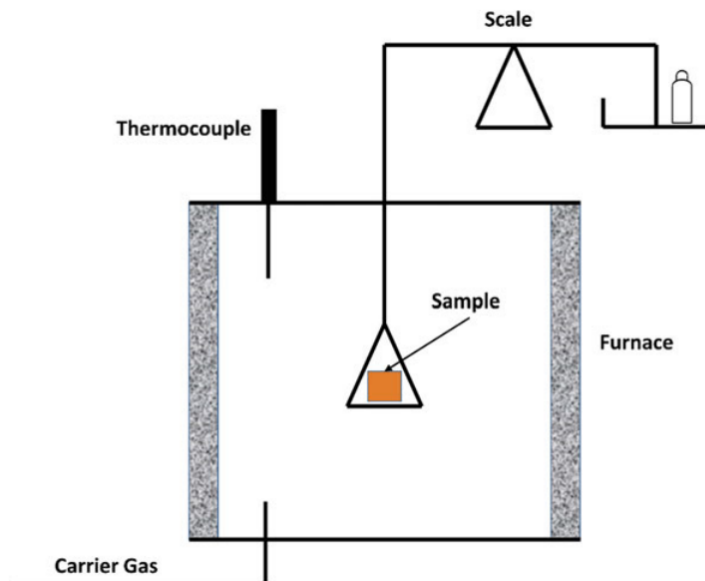
Figure 2.5: Schematic representation of thermogravimetric method. Recovered from the reference[30]

In previous works, TGA technique was used to study the thermal stability of PVP and composite fibers[31,32]. PVP fibers were analyzed using a temperature range from O to 850°C while CNTs/PVP composite was from O to 600°C. Both cases was done in N_2 atmosphere with heating rate of 10°C/min[31,32].

2.5.3   Fourier Transform Infrared Spectroscopy (FTIR)

Fourier Transform Infrared has been used to analyze materials for over 70 years. Concerning IR spectroscopy, IR radiation passes through a sample where some IR radiation is absorbed and transmitted, creating a molecular fingerprint of the sample (spectrum)[33]. This spectrum is composed of absorption peaks representing vibration frequencies between the atom bonds of the material[33]. Moreover, to identify an organic compound, it is necessary to match a reference IR spectrum with an unknown compound. For that reason, the following equation[33] is used

$$A = log_{10}\left(\frac{1}{T}\right) = -log_{10}(T) = -log_{10}\left(\frac{1}{I_o}\right), \tag{2.1}$$

where T is the transmittance, I is the radiant power, I_o is the radiant power incident on the sample, and A is the absorbance.

FTIR working principle is divided in[33]:

1. The source: IR energy is emitted from a glowing blackbody source, in which the amount of incident energy can be controlled by an aperture.

2. The interferometer: The beam enters the interferometer where the "spectral encoding" occurs.

3. The sample: The beam enters the sample compartment where the beam is transmitted or reflected.

4. The detector: The beam that passes is measured by the detector.

5. Reflection gratings: A prism is used to reduce the effect of overlapping and stray radiation.

6. Mirror: Mirrors help to focus the IR radiation.

7. Windows and computer: Together, help to digitize the signals to obtain the IR spectrum.
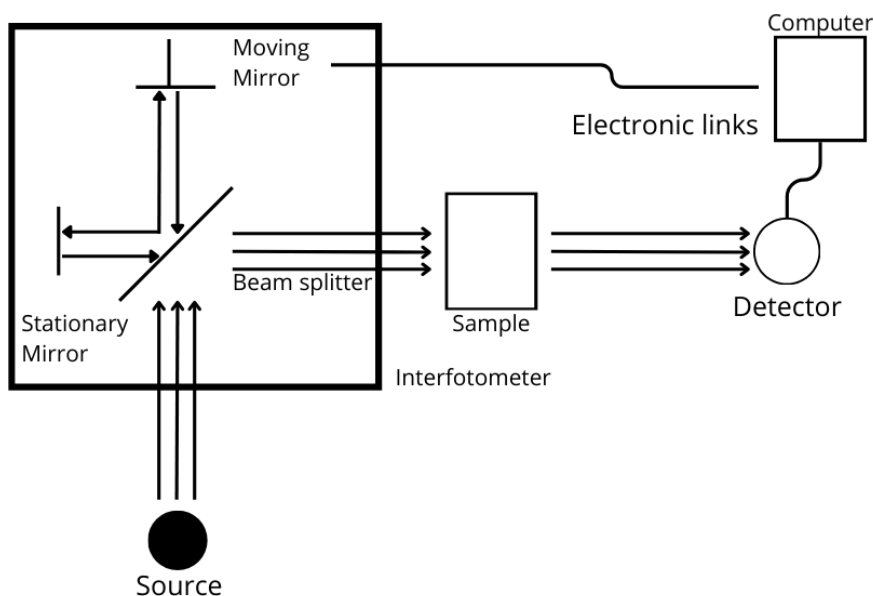
Figure 2.6: Schematic representation of FTIR instrument[33].

An analysis of vibration frequencies between atom bonds is crucial to obtain a molecular fingerprint because peak positions depend specifically on functional groups in the molecules, making it relevant to characterize composite materials. Omran et al. (2021) studied the streching and bending vibration bands of MWCNTs within the PVP matrix by FTIR technique with a wavenumber range from 400 to 4000 cm^{-1} [34]. Stobinski et al. (2010) mention that MWCNTs spectrum shows a peak at ~3444 cm^{-1} which corresponds to OH stretching, and in the range of 1750-1550 cm^{-1}, C=O vibrational mode is found. Moreover, the C=C streching and C-O vibrational mode are located at ~1640 and ~1550 cm^{-1}, respectively[35].

Finally, Annette, Sudhakar, Ursula and Andrea[36,37] showed the applicability of FTIR for natural fibre studies as can seen in the figure 2.7[38].

Peak wavenumber (without dislocation) (cm⁻¹)	Peak wavenumber (with dislocation) (cm⁻¹)	Δv(cm⁻¹)	Bonds
3327	3332	5	OH stretching
2883	2882	-1	C–H symmetrical stretching
1724	1724	0	C=O stretching vibration
1623	1624	1	OH bending of absorbed water
1506	disappear	-	C=C aromatic symmetrical stretching
1423	1423	0	HCH and OCH in-plane bending vibration
1368, 1363	1367,1363	-1/0	In-the-plane CH bending
1325	1325	0	S ring stretching
1314	1313	-1	CH₂ rocking vibration at C6
1259	1261	1	G ring stretching
1245	1244	-1	C-C plus C-O plus C=O stretch; G condensed > G etherfied
1232	1231	-1	COH bending at C6
1204	1199	-5	C-O-C symmetric stretching, OH plane deformation
1152	1156	4	C-O-C asymmetrical stretching
1046	1043	-3	C-C, C-OH, C-H ring and side group vibrations
1020	1018	-2	C-C, C-OH, C-H ring and side group vibrations
994	996	2	C-C, C-OH, C-H ring and side group vibrations
895	894	-1	COC,CCO and CCH deformation and stretching
662	663	1	C-OH out-of-plane bending

Figure 2.7: Bonds wavenumber related to regions without and with dislocations of natural fibers. Recovered from[38]

2.5.4   Raman Spectroscopy

In 1923, Smekal postulated the phenomenon of inelastic scattering of light; however, it could be observed experimentally in 1928 by Raman and Krishnan[39]. The fundamental base of Raman spectroscopy is the interaction of light with the matter in which the photons that make up the light may be absorbed, scattered or not interact with the material[39]. A photon is absorbed when an incident photon of light corresponds to an energy gap between the ground state and an excited state[39]. It makes the molecule jump up to a higher energy excited state, making this interaction be measured by detecting the loss of that energy of radiation from the light[39]. Moreover, this radiation could be analyzed and discussed in energy terms.

$$\lambda = c/v, \tag{2.2}$$

where λ is the radiation expressed in terms of wavelength, c is the speed of light, and v is the frequency. Finally,

$$v = \Delta E/h, \tag{2.3}$$

$$\varpi = v/c = 1/\lambda \tag{2.4}$$

Considering these equations, it is clear that the energy (ΔE) is inversely proportional to the wavelength (λ). The radiation is employed in Raman spectroscopy because it uses a single frequency of radiation to irradiate the sample[39]. At that moment, one vibrational unit of energy different from incident light is detected.

It is important to consider that there is no change in electronic energy in molecular vibrations[39]. For instance, concerning the absorption of a photon and the jump up of an electron to an excited electronic state, the molecule energy can be divided into degrees of freedom. With three of these degrees of freedom, the translation of the molecule in space can be described, and with three more, the rotational movement, except for linear molecules, can also be described[39]. Therefore, considering N is the number of atoms in a molecule, the number of vibrations possible (freedom vibrational degrees number) is 3N-6 for all molecules, except for linear ones, which is 3N-5[39]. Furthermore, it is known that there is only one vibration in a diatomic molecule, but a triatomic molecule will have three modes of vibrations, as can be observed in figure 2.8. Spring and ball model is widely used to interpret vibrational spectra[39].
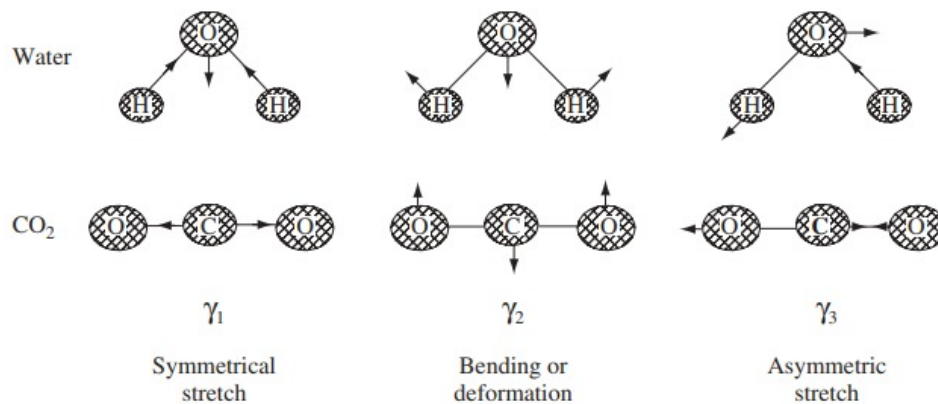
Figure 2.8: Vibration modes of H_2O and CO_2 by Spring and ball model. Recovered from[39]

Therefore, analyzing modes of molecule vibrations makes Raman spectroscopy a powerful technique for quality dispersion characterization of MWCNTs-based composite[40]. Nasouri et al. (2017) mention that MWCNTs consist of three characteristic main bands: D-band at ~1330 cm^{-1}, the G-band at ~1590cm^{-1} and the G'-band at ~2715 cm^{-1} [40].

Chapter 3

Methodology

3.1 Materials and reagents

Polyvinylpyrrolidone (PVP) (Mw 30 000 gmol^{-1}, Mw 40 000 gmol^{-1}, and Mw 1 300 000 gmol^{-1}) and N,N-Dimethylformamide (99.9% purity) were obtained from Sigma and Aldrich Co. The commercial multi-wall carbon nanotubes were obtained from Elicarb MW (Dry). The reagents used in the cobalt ferrite synthesis were iron acetylacetonate, cobalt acetylacetonate, 1,2 hexadecanediol, oleic acid, oleylamine, benzyl ether, were of analytical grade and used without further purification.

3.2 Methods

3.2.1 Preparation of PVP solutions

Polyvinylpyrrolidone (Mw 30000 gmol^{-1}) was prepared with 0.5 and 0.6 g of PVP flakes added to 4.5 and 4.4 mL of ethanol, respectively. PVP samples were stirred at 500 rpm for 30 min at room temperature until homogeneous solutions were obtained at 10 and 12 wt%, respectively. PVP (Mw 40000 gmol^{-1}) of 10 and 12 wt% were obtained with PVP flakes (0.5 and 0.6 g) added to 4.5 and 4.4 mL of N,N-dimethylformamide (99.9% purity). PVP samples were dissolved at room temperature under low agitation for 30 min to obtain homogeneous solutions. PVP (Mw 1300000 gmol^{-1}) was prepared with 5 g of PVP flakes added to 45 mL of ethanol and stirred at 500 rpm for 30 min at room temperature to obtain a homogeneous solution of PVP at 10 wt%. The PVP processes are represented in the figure 3.1.
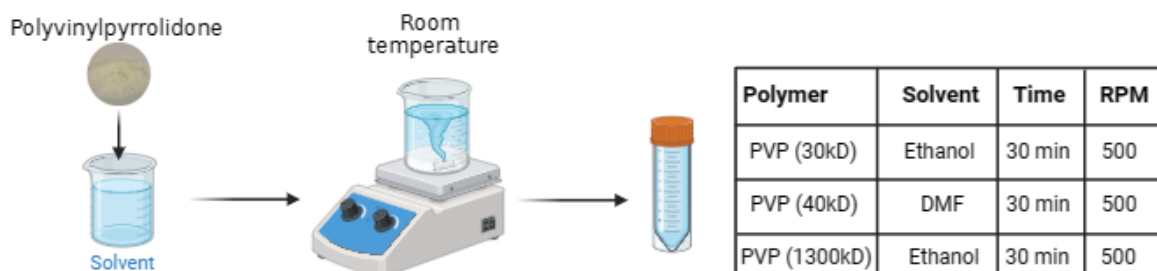
Figure 3.1: Schematic representation of PVP solutions at different molecular weights.

3.2.2   Synthesis of CoFe$_2$O$_4$ nanoparticles.

Co(acac)3 (1 mmol), Fe(acac)3 (2 mmol), 1,2-hexadecanediol (10 mmol), oleic acid (6 mmol), oleylamine (6 mmol), and phenyl ether (20 mL) were mixed and magnetically stirred. The mixture was heated to 200 °C for 30 minutes and then to reflux (265 °C) for another 30 minutes. The black-brown mixture was cooled to room temperature by removing the heat source. Under ambient conditions, ethanol (40 mL) was added to the mixture, and a black material was precipitated and separated via centrifugation.

To prepare the sample CoFe$_2$O$_4$ (10 nm), 84 mg of CoFe$_2$O$_4$ previously prepared nanoparticles dispersed in hexane (4 mL) was added, and the mixture was heated to 200 °C for 30 min and then, heated to reflux (265 °C) for another 30 min. The black-brown mixture was cooled to room temperature by removing the heat source. Under ambient conditions, ethanol (40 mL) was added to the mixture, and a black material was precipitated and separated via centrifugation. The same process was repeated using the previous core for the 15, 20, and 25 nm samples.

3.2.3   Preparation of PVP/CoFe$_2$O$_4$ composite

PVP/CoFe$_2$O$_4$ composite was prepared using 0.3 mL of CoFe$_2$O$_4$ nanoparticles (size = 5, 10, 15, 20, and 25 nm) were added to 2.7 mL of PVP (Mw 1300000 gmol^{-1}) (10 wt%) in ethanol. To obtain a homogeneous solution, the PVP/CoFe$_2$O$_4$ sample was sonicated for 3 minutes 50 seconds with a 90% amplitude as can be seen in the figure 3.2.

3.2.4   Preparation of PVP/MWCNT composite

PVP/MWCNT composite was prepared using 0.3 mL of MWCNT (0.001g) was mixed with 2.7 mL of PVP (Mw 1300000 gmol^{-1}) (10 wt%) in ethanol, and then the solution was sonicated for 4 minutes 30 seconds with a 90% amplitude to obtain a homogeneous solution (Fig.3.2).

3.2.5   Preparation of PVP/MWCNT/CoFe$_2$O$_4$ composite

PVP/MWCNT/CoFe$_2$O$_4$ composite was prepared using 0.3 mL of MWCNT (0.001g)/CoFe$_2$O$_4$ nanoparticles (size = 5, 10, 15, 20 and 25 nm) were added to 2.7 mL of PVP (Mw 1300000 gmol^{-1}) (10 wt%) in ethanol. The solution was sonicated for 3 to 4 minutes with a 90% amplitude until a homogeneous solution (Fig.3.2).
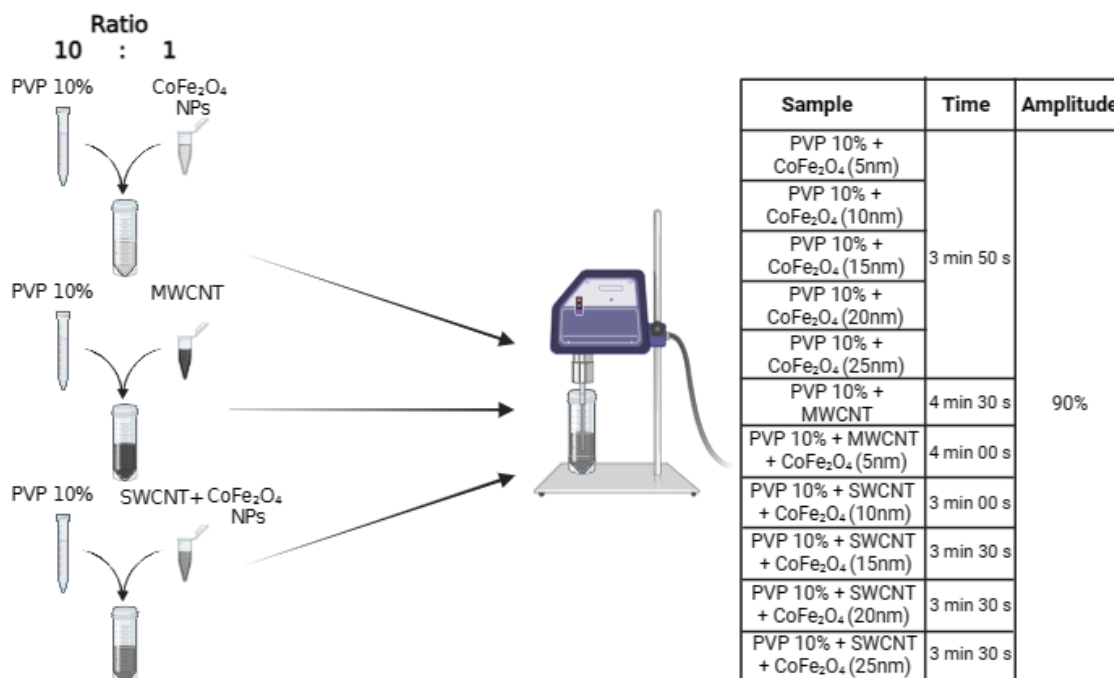
Figure 3.2:   Schematic   representation   of   the   process   of   PVP/CoFe$_2$O$_4$,   PVP/MWCNT,   and PVP/MWCNT/CoFe$_2$O$_4$ composites using PVP (Mw 1 300 000) at 10 wt%.

3.2.6   Electrospinning of PVP, PVP/CoFe$_2$O$_4$, PVP/MWCNT, and PVP/MWCNT/CoFe$_2$O$_4$ composite.

PVP, PVP/CoFe$_2$O$_4$, PVP/MWCNT, and PVP/MWCNT/CoFe$_2$O$_4$ fibers were fabricated using *SprayBase^{TM}* electrospinning technique. The *SprayBase^{TM}* electrospinning equipment consists of three primary parts: a solution release system, a power supply, and a collector. The nanofibers were deposited onto an aluminum foil, which was the collector. A DC voltage supply was used to release the PVP solutions at a controlled flow rate between 0.010 mL/h and 0.500 mL/h. An electrical potential was applied to solutions to evaporate the solvents. It was under a high electric voltage ranging from 3.80 kV to 13.84 kV power source. The distance between the emitter and collector was between 9 and 14 cm. The diameters of emitters used were 0.35 and 0.55 (24G). The electrospinning process was realized under room temperature (16°C). The specific parameters used for each solution are shown in tables 3.1 and 3.2.

Figure 3.3: *SprayBase^{TM}* electrospinning equipment and setup.

Solution	Concentration	Flow rate	Voltage	Distance	Emitter
Polymer/Solvent	(%)	(mL/h)	(kV)	(cm)	diameter (mm)
PVP (30 000 g/mol) /	10	0.500	13.84	9	0.45
Ethanol	12	0.400	12.51	9	0.35
PVP (40 000) /	10	0.350	8.42	9	0.45
DMF	12	0.350	6.63	9	0.45
PVP (1 300 000)/ Ethanol	10	0.150	6.00	13	0.55

Table 3.1: Electrospinning parameters of PVP solutions.

Sample	Syringe volume (mL)	Flow rate (mL/h)	Voltage (kV)	Distance (cm)	Emitter diameter (mm)
PVP (10 wt%) / CoFe$_2$O$_4$ (5nm)	3	0.500	3.95	13	0.55
		0.150	4.50	14	
		0.010	4.60	13	
		0.015	4.00	13	
		0.050	4.30	13	
PVP (10 wt%) / CoFe$_2$O$_4$ (10nm)	3	0.050	4.00	14	0.55
PVP (10 wt%) / CoFe$_2$O$_4$ (15nm)	3	0.050	3.40	14	0.55
PVP (10 wt%) / CoFe$_2$O$_4$ (20nm)	3	0.050	3.81	14	0.55
PVP (10 wt%) / CoFe$_2$O$_4$ (25nm)	3	0.050	4.05	13.5	0.55
			4.00	14	
PVP (10 wt%) / MWCNT	3	0.030	4.50	14	0.55
PVP (10 wt%) / MWCNT/ CoFe$_2$O$_4$ (5nm)	10	0.030	4.50	14	0.55
		0.050	4.25	14	
PVP (10 wt%) / MWCNT/ CoFe$_2$O$_4$ (10nm)	10	0.050	4.00	14	0.55
		0.050	3.75	13	
		0.020	3.75	14	
PVP (10 wt%) / MWCNT/ CoFe$_2$O$_4$ (15nm)	10	0.020	3.80	14	0.55
PVP (10 wt%) / MWCNT/ CoFe$_2$O$_4$ (20nm)	3	0.020	4.10	14	0.55
PVP (10 wt%) / MWCNT/ CoFe$_2$O$_4$ (25nm)	3	0.020	4.10	14	0.55
		0.025	4.10	14	

Table 3.2: Electrospinning parameters of PVP/CoFe$_2$O$_4$, PVP/MWCNT, and PVP/MWCNT/CoFe$_2$O$_4$ samples using the PVP (Mw 1 300 000) at 10 wt%.

3.2.7 Fabrication of interdigitated circuit

The fabrication of interdigitated circuits began by cutting twelve 8 x 5 cm bakelite plates (a). After, an interdigitated design was printed onto photographic paper and stamped onto the bakelite plates. Heat and pressure were applied using a clothes iron for 5 minutes to transfer the design onto the plates. Then, the plates were introduced in water for 7 minutes to remove the paper easily (b). After that, stamped bakelite plates were introduced in ferric chloride until the copper exposed was removed (etching process)(c). Again, devices were put in water to clean the ferric chloride, and finally, printing ink was removed by thinner (d), as can seen in the figure 3.4
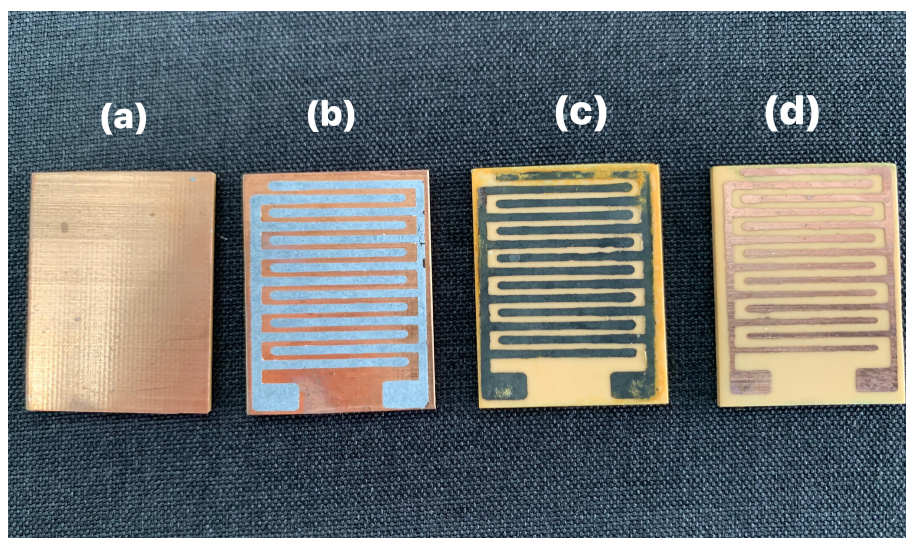
Figure 3.4: Interdigitated circuit process (a) 8 x 5 cm bakelite plate, (b) electrodes mask printed, (c) after etching process and (d) interdigitated circuit device.

3.2.8 Fibers deposition on interdigitated devices

Once interdigitated devices were fabricated, the oxide in the surface was removed using sandpaper (grain number 1200). After that, the devices were sonicated in acetone, 2−propanol, and distilled water in an ultrasonic bath for 10 minutes, respectively. Then, nitrogen gas was used to remove the water residues of the devices. Next, a Kapton film was used to create a mask and determine the region where fibers would be deposited. Finally, interdigitated devices were put into the electrospinning equipment, and fibers were deposited (Fig.3.5). Each solution's deposition time is shown in the table 3.3.

Solution	Flow rate (mL/h)	Deposition time (min)	Deposition volume (mL)
PVP 10 wt%	0.150	25	0.0625
PVP 10 wt% / $CoFe_2O_4$ (5nm)	0.015	250	0.0625
PVP 10 wt% / $CoFe_2O_4$ (10nm)	0.050	75	0.0625
PVP 10 wt% / $CoFe_2O_4$ (15nm)	0.050	75	0.0625
PVP 10 wt% / $CoFe_2O_4$ (20nm)	0.050	75	0.0625
PVP 10 wt% / $CoFe_2O_4$ (25nm)	0.050	75	0.0625
PVP 10 wt% / MWCNT	0.030	125	0.0625
PVP 10 wt% / MWCNT / $CoFe_2O_4$ (5nm)	0.020	187	0.0625
PVP 10 wt% / MWCNT / $CoFe_2O_4$ (10nm)	0.020	187	0.0625
PVP 10 wt% / MWCNT / $CoFe_2O_4$ (15nm)	0.020	187	0.0625
PVP 10 wt% / MWCNT / $CoFe_2O_4$ (20nm)	0.020	187	0.0625
PVP 10 wt% / MWCNT / $CoFe_2O_4$ (25nm)	0.020	187	0.0625

Table 3.3: Deposition times of each solution remaining constant to deposition volume.
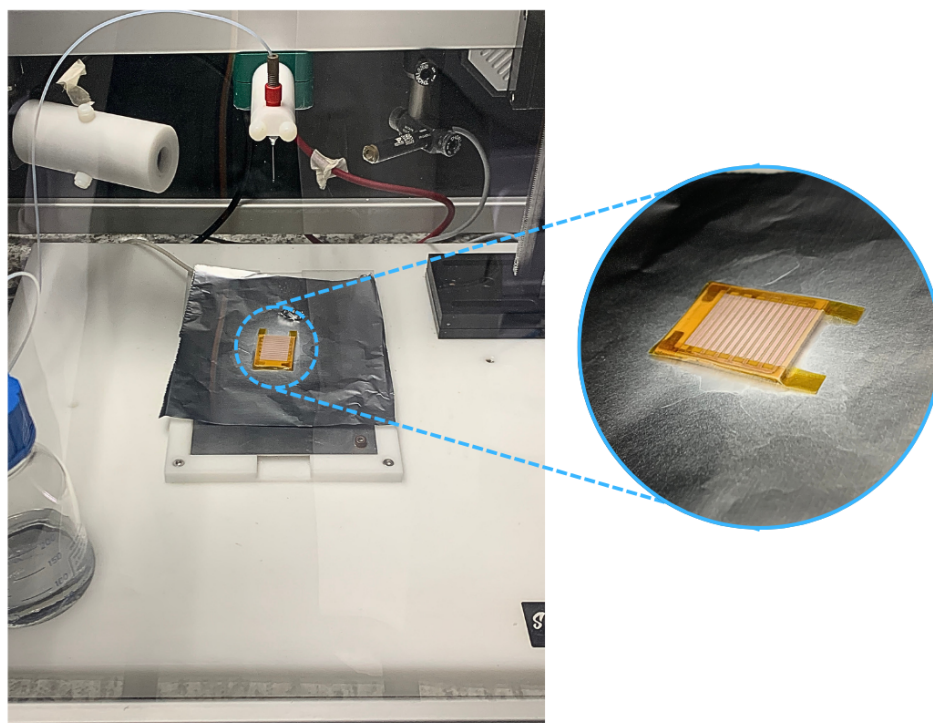
Figure 3.5: An interdigitated device with fibers deposited into electrospinning equipment. A Kapton film (yellow) was used to determine the deposition region.

3.3 Characterization

3.3.1 Optical Microscopy

The optical images were taken using an optical microscope from Raman equipment. The magnification range was from 50 to 100 x. Each sample was observed at different points to analyze the size distribution.
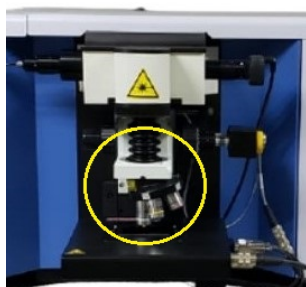
Figure 3.6: Optical microscope integrated to Raman equipment.

3.3.2 Thermogavimetric Analysis (TGA)

TGA characterization was carried out using TA TGA 55. This equipment is located in the School of Chemical Sciences and Engineering Laboratory at Yachay Tech University. TGA measurements were made using nitrogen gas with a temperature range of 0 to 800°C, and a ramp temperature of up to 20°C/min.

Figure 3.7: Thermogravimetric analyzer, TGA 55

3.3.3   Fourier Transform Infrared Spectroscopy (FTIR)

FTIR characterization was made by AGILENT Cary-630 Fourier transform infrared spectrometer. FTIR measurements were made in a range from 4000 to 500 cm^{-1}.

Figure 3.8: FTIR spectrometer, AGILENT Cary-630

3.3.4   Raman Spectroscopy

The Raman spectroscopy analysis for all samples was taken by LabRam HR Evolution microscope, located in the laboratory of characterization of the School of Physical Sciences and Engineering at Yachay Tech University, Ecuador. To characterize, fibers were deposited in different glass slides using the following parameters: a) wavenumber range from -20 to 3200 cm^{-1}, b) the laser was 633 nm with a power of 50% , and c) acquiring time was set to 20 seconds with 5 five accumulations per measurement.
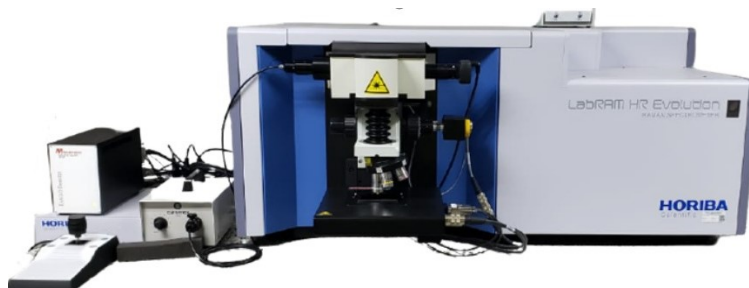
Figure 3.9: Raman spectrometer, HORIBA LabRAM HR Evolution

3.3.5   Voltage vs Resistance

The equipment consists of a DC power supply (V_o), a safety resistor (R1), a multimeter (with its internal resistance RM), and a device that would be measured (Interdigitated circuit) (Rx). The applied voltage range was 421 to 100 V, R1 was 1.18 MΩ, and RM was 10 MΩ. The measurement setup and equipment are shown in the figures 3.10 and 3.11, respectively.
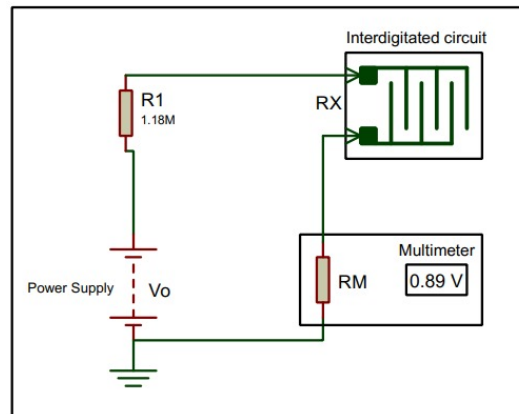
Figure 3.10: Circuit diagram of the measurement setup
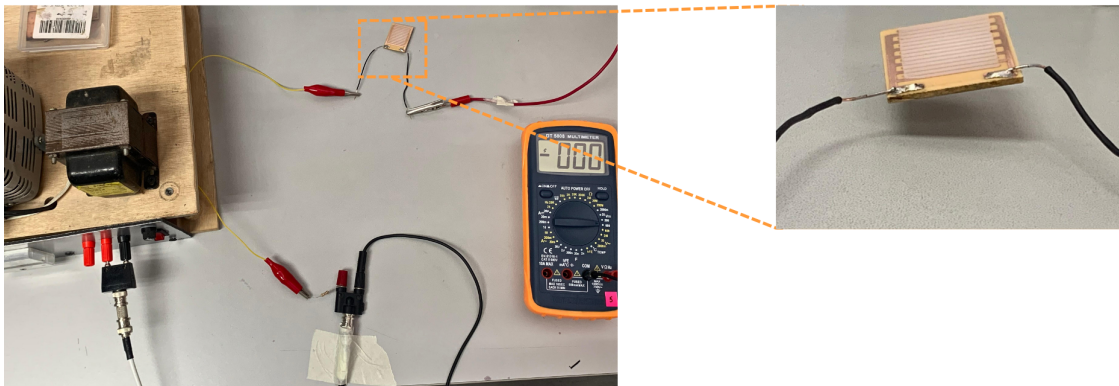
Figure 3.11: Homemade measurement equipment

As can be seen, the homemade equipment is connected in series. The resistance of the material is

calculated by the following equation:

$$R_X = R_M \left(\frac{V_o}{V_f} - 1 \right) - R_1, \tag{3.1}$$

where R_X is the calculated resistance, R_M is the internal resistance of multimeter, V_o is the applied voltage, V_f is the output voltage in the multimeter, R_1 is the safety resistor of 1.18MΩ.

Chapter 4

Results & Discussion

Section 4.1 analyzes parameters that affect the electrospinning process using PVP polymer. Factors such as molecular weight, solution concentration, and working parameters are discussed. Section 4.2 shows the structure of the fiber through optical microscopy and explains the spectra from Raman Spectroscopy, FTIR, and TGA. Section 4.3 exhibits an analysis of applied voltage against the resistance of fibers of PVP and composites.

4.1   Electrospinning parameters optimization

The electrospinning technique is a powerful tool to fabricate new materials for several applications, from textiles to electronic devices. These applications depend on three important conditions: a) the molecular weight of the polymer, b) solution concentration, and c) the working parameters of electrospinning equipment. This study used PVP polymers at three different molecular weights: 30 000, 40 000, and 1 300 000 g/mol. Once the PVP solutions were prepared, they were put into electrospinning equipment to find each parameter, as shown in Table 3.1. Figure 4.1a shows an electrospray formation. The droplet carries a charge distributed over its surface, leading to a Coulombic repulsion force. It makes an unstable droplet, breaking into smaller droplets[41]. This behavior was characteristic of PVP at molecular weights of 30,000 and 40,000 g/mol. Figure 4.1b exhibits an electrospinning formation where the applied voltage produces an electric force on the fluid droplet, forming a Taylor cone[42]. It makes the solvent evaporate fast, producing an elongated jet. This behavior was obtained by PVP at a molecular weight of 1 300 000 g/mol and composites solutions. Therefore, the molecular weight is the crucial difference between electrospraying and electrospinning, as Li et al. (2021) mentioned[42].

(a) Electrospraying   (b) Electrospinning
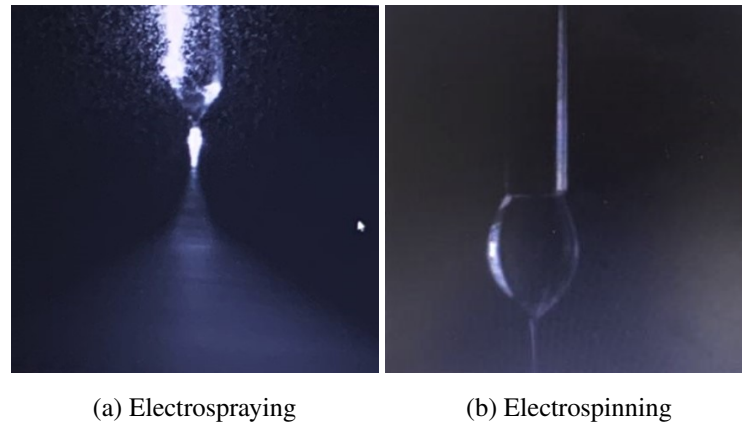
Figure 4.1: Electrospraying and electrospinning process

Figure 4.2 illustrates the Taylor cone formation necessary to fabricate fibers. Firstly, a PVP solution is added, forming a spherical droplet. Then, a charge is applied to the fluid droplet, stretching into an ellipsoid shape to maintain the force balance[42]. When the optimal applied voltage is found, the Taylor cone is formed, producing jet elongations (fibers)[42,43]. To achieve consistent fiber fabrication, maintaining a sufficient amount of liquid to support the ejected amount during the electrospinning process[42]. Nevertheless, when the applied voltage achieves the critical voltage, the balance of repulsive forces is broken, producing flow instability and forming random fibers without a controlled diameter[41,42]. Thus, the applied voltage influences the formation of fibers in the electrospinning process[42].
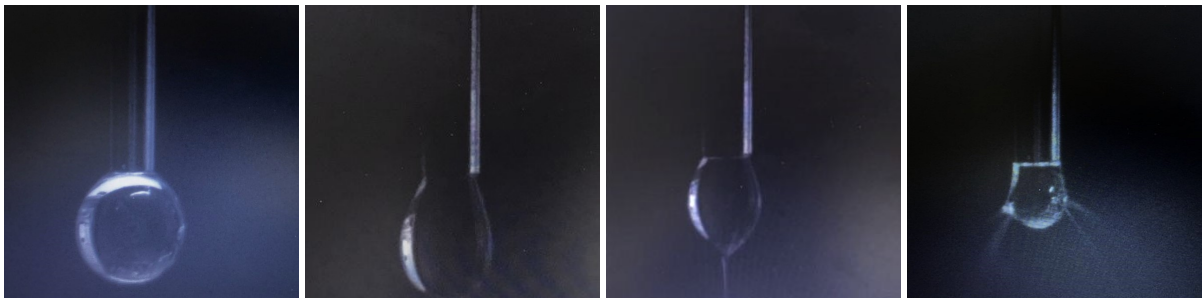
(a) Formation of a PVP droplet   (b) Formation of an elongated PVP droplet   (c) Correct formation of Taylor cone   (d) Flow instabilities in the needle tip

Figure 4.2: The influence of input voltage for the formation on Taylor cone

4.2 Structural and composition characterization

4.2.1 Optical Microscopy

Once the fibers were fabricated using the electrospinning technique, they were characterized by optical microscopy to observe their morphology. Figure 4.3a shows PVP fibers free from beads, indicating that polymer concentration was sufficient in the precursor solution for the electrospinning process [44] (optimal parameter). These fibers have a smooth appearance with an average diameter of 4.13 μm (Fig.4.4a). Figure 4.3b also exhibits PVP/CoFe$_2$O$_4$(5nm) fibers free from beads with an average diameter of 2.23 μm (Fig.4.4b); however, some tiny drops are present. The fibers of PVP/CoFe$_2$O$_4$(10nm) and PVP/CoFe$_2$O$_4$(15nm) are aligned and free from beads (Fig.4.3c,d) with an average diameter of 1.20 and 1.82 μm (Fig.4.4c,d), respectively. Figure 4.3e also shows PVP/CoFe$_2$O$_4$(20nm) fibers free from beads with a combination of align and spiral fibers. Additionally. The fibers' average diameter is 2.29 μm (Fig.4.4e). The PVP/CoFe$_2$O$_4$(25nm) fibers are free from beads (average diameter=1.95μm, Fig.4.4f), but there is a big drop between them, which could affect the flow of electrons(Fig.4.3f). The PVP/MWCNTs fibers are free from beads and have an aligned behaviour(Fig.4.3g) due to the electrical properties of carbon nanotubes. Moreover, these fibers have an average diameter of 2.11 μm (Fig.4.5g). The fibers of PVP/MWCNT/CoFe$_2$O$_4$(5nm), PVP/MWCNT/CoFe$_2$O$_4$(10nm) and PVP/MWCNT/CoFe$_2$O$_4$(20nm) are free from beads in which the majority of fibers are not aligned (Fig. 4.3h,i,k) with an average diameter of 0.55, 0.68, 0.55 μm (Fig.4.5h,i,k) while the PVP/MWCNT/CoFe$_2$O$_4$(15nm) and PVP/MWCNT/CoFe$_2$O$_4$(25nm) fibers have an aligned behavior (Fig.4.3j,l) with an average diameter of 1.07 and 1.05 μm (Fig.4.5j,l), respectively.

To make a general fiber diameter analysis, it is necessary to consider four principal groups with their average diameter: a) PVP (4.13μm), b) PVP/CoFe$_2$O$_4$ (1.90μm), c) PVP/MWCNTs (2.11μm) and d)PVP/MWCNTs/CoFe$_2$O$_4$ (0.78μm). There are remarkable size reductions against the PVP fibers. It agrees with Lamastra et al.[45], which explains that this effect is associated with the conductivity properties of MWCNTs and CoFe$_2$O$_4$. Nevertheless, PVP/MWCNTs have an average diameter higher than PVP/MWCNTs/CoFe$_2$O$_4$ and PVP/MWCNTs/CoFe$_2$O$_4$. Nasouri et al.[40] reports that the increment of diameter of PVP/MWCNTs is due to the concentration of MWCNTs in PVP due to the viscosity of the solution increases when the concentration increases. As literature described[40], when the viscosity of electrospinning solution increases, the diameter of fiber increases too[40].

(a) PVP 10 wt%

(b) PVP/CoFe$_2$O$_4$(5nm)

(c) PVP/CoFe$_2$O$_4$(10nm)

(d) PVP/CoFe$_2$O$_4$(15nm)

(e) PVP/CoFe$_2$O$_4$(20nm)

(f) PVP/CoFe$_2$O$_4$(25nm)

(g) PVP/MWCNT

(h) PVP/MWCNT/CoFe$_2$O$_4$(5nm)

(i) PVP/MWCNT/CoFe$_2$O$_4$(10nm)

(j) PVP/MWCNT/CoFe$_2$O$_4$(15nm)

(k) PVP/MWCNT/CoFe$_2$O$_4$(20nm)

(l) PVP/MWCNT/CoFe$_2$O$_4$(25nm)
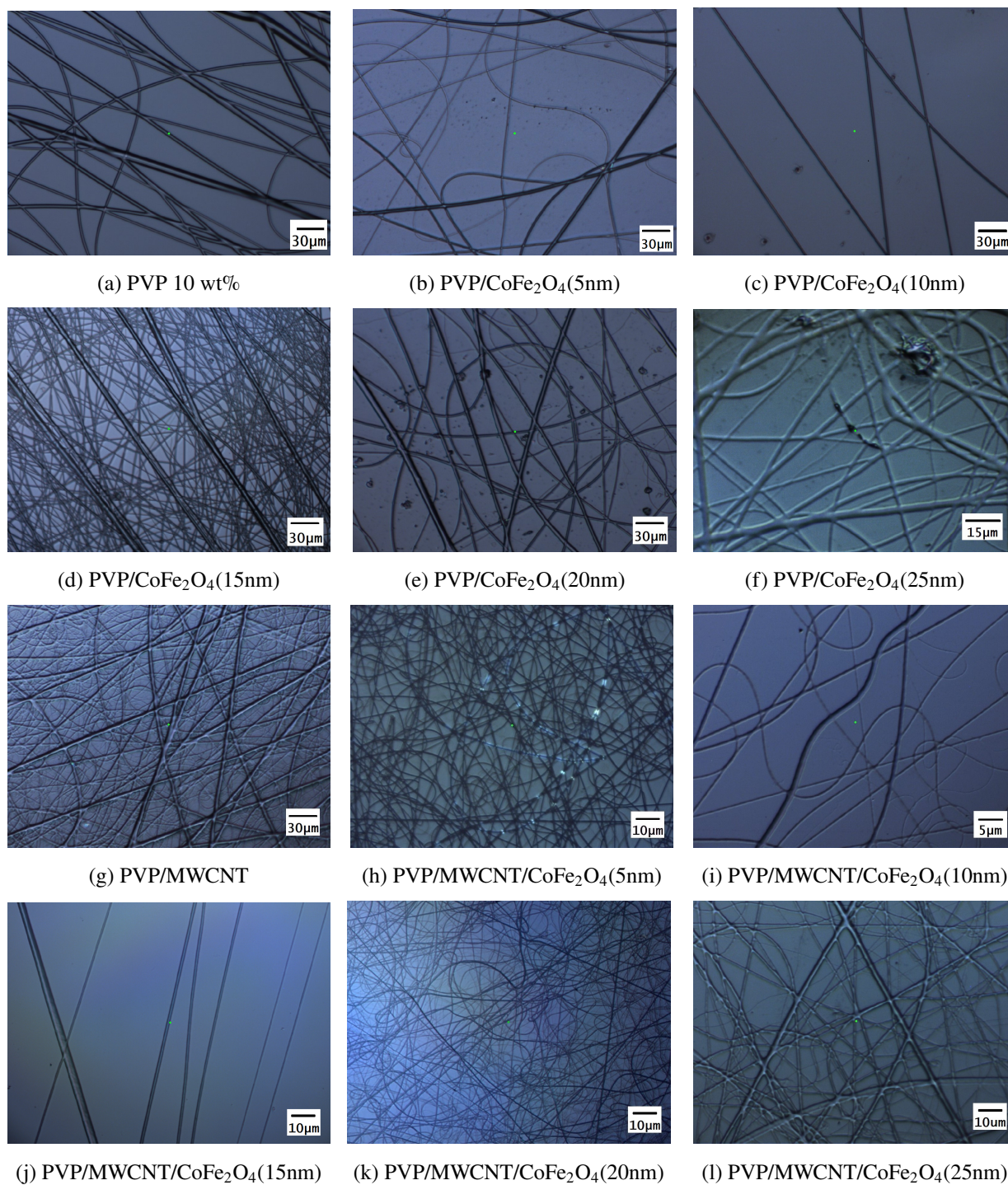
Figure 4.3: Optical images of PVP, PVP/CoFe$_2$O$_4$, PVP/CNT and PVP/CNT/CoFe$_2$O$_4$ fibers.
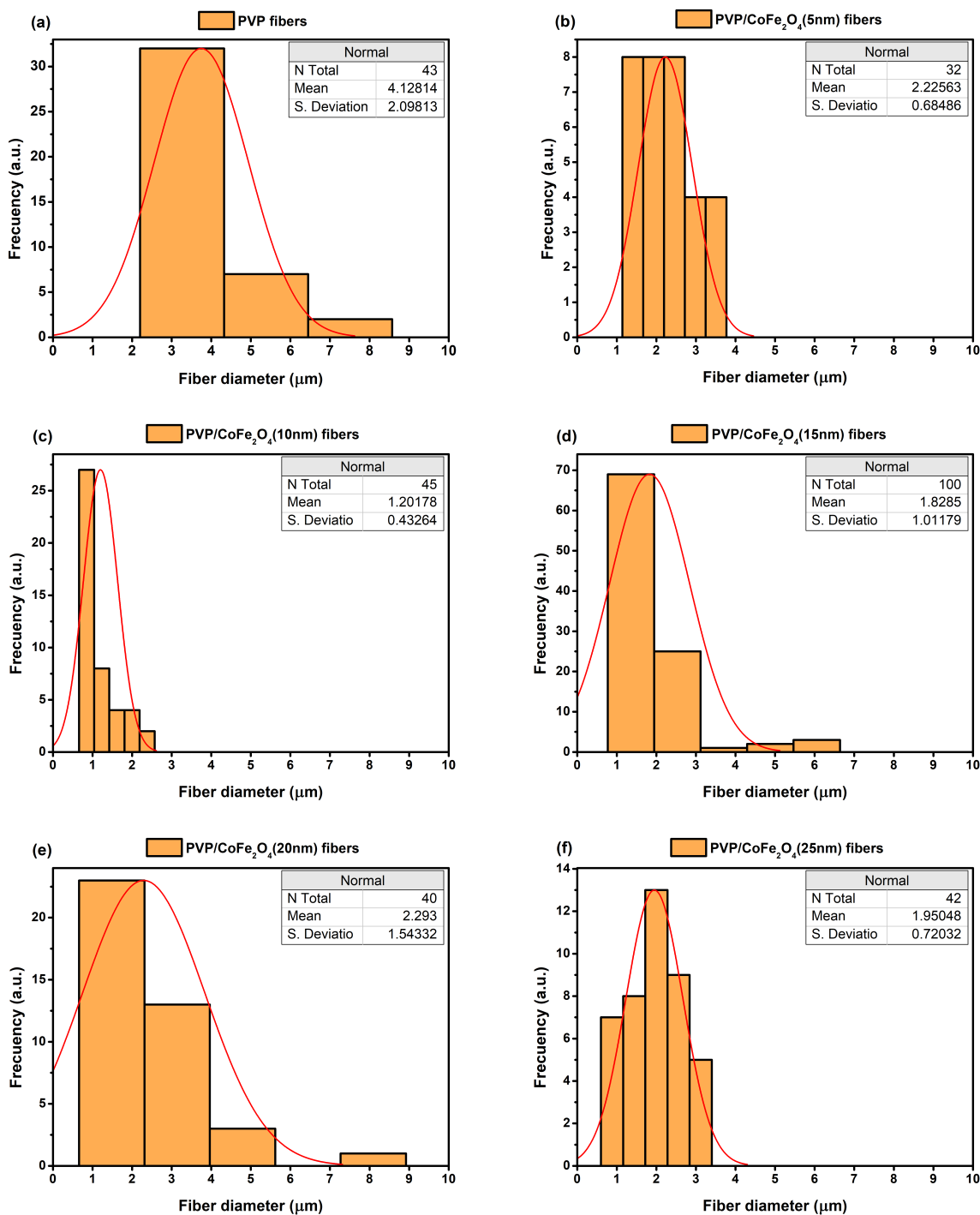
Figure 4.4: Fiber diameter histograms: a) PVP, b) PVP/CoFe$_2$O$_4$ (5nm), c) PVP/CoFe$_2$O$_4$ (10nm), d) PVP/CoFe$_2$O$_4$ (15nm), e) PVP/CoFe$_2$O$_4$ (20nm) and f) PVP/CoFe$_2$O$_4$ (25nm).
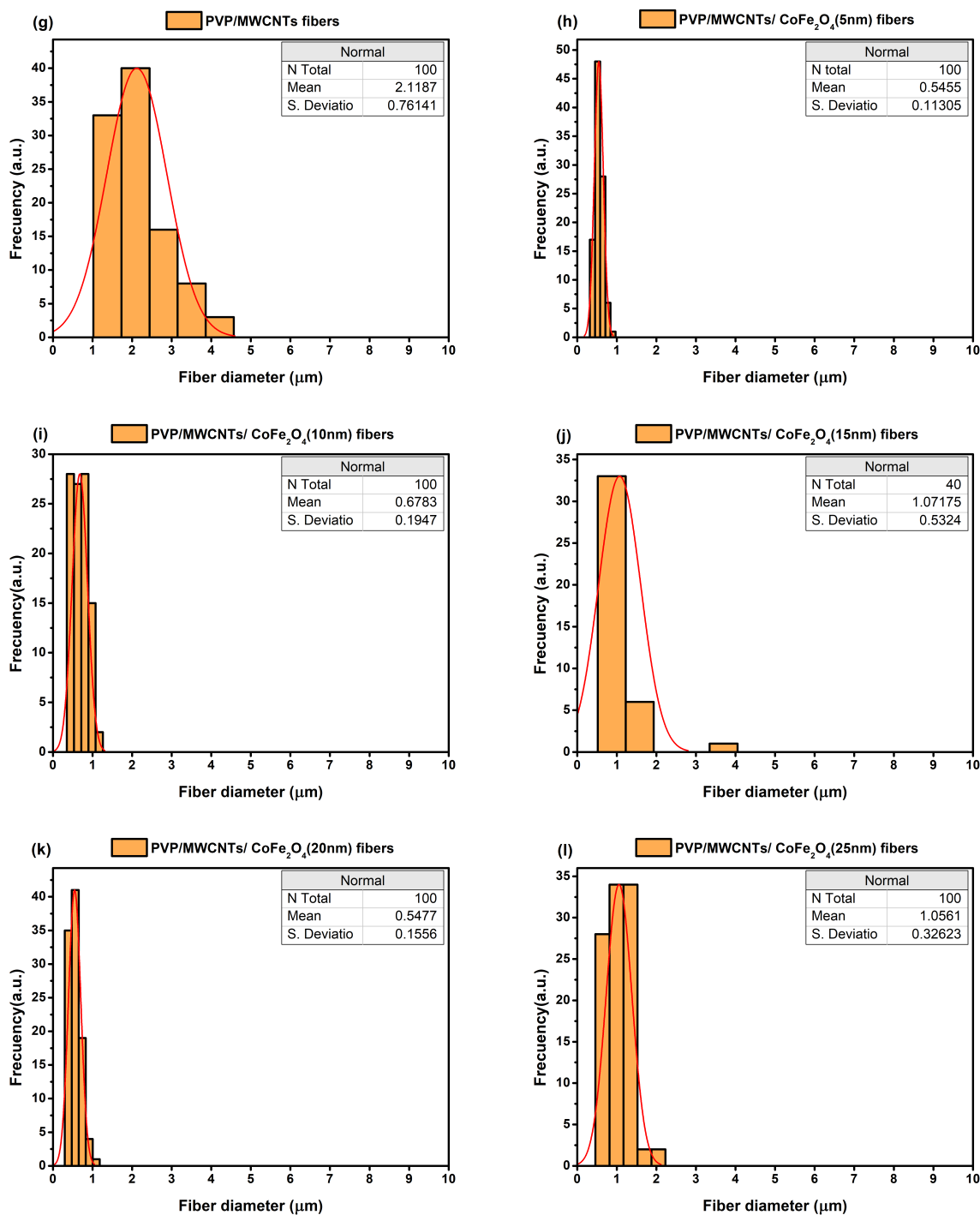
Figure 4.5: Fiber diameter histograms: g) PVP/MWCNTs, h) PVP/MWCNTs/CoFe$_2$O$_4$ (5nm), i) PVP/MWCNTs/CoFe$_2$O$_4$ (10nm), j) PVP/MWCNTs/CoFe$_2$O$_4$ (15nm), k) PVP/MWCNTs/CoFe$_2$O$_4$ (20nm), l) PVP/MWCNTs/CoFe$_2$O$_4$ (25nm).

4.2.2 Raman Spectroscopy

Figure 4.6 shows the Raman spectra of PVP fibers, PVP/CoFe$_2$O$_4$ fibers, PVP/MWCNT fibers, and PVP/MWCNT/CoFe$_2$O$_4$ fibers. PVP spectrum of pure PVP fibers (a) shows peaks at 2928, 1670, 1450, and 1232 cm^{-1} are attributed to C–H stretching, C=O stretching, CH$_2$ scissor vibration, and CH$_2$ twisting vibration, respectively. These peaks are consistent with other research for PVP[46,47]. The PVP/CoFe$_2$O$_4$ fibers spectrum (b) has the same behavior that the PVP fibers (black line) spectrum due to the very low concentration of CoFe$_2$O$_4$ nanoparticles, making that PVP spectrum overlap the peaks of CoFe$_2$O$_4$ nanoparticles. PVP/MWCNT spectrum (c) exhibits 2 well-defined peaks at 1329 and 1590 cm^{-1} are associated with D-band($\sim$ 1330 cm^{-1}) and G-band ($\sim$ 1590 cm^{-1}), respectively[40]. The D-band usually indicates the presence of defects as amorphous carbon (carbonaceous impurities with sp^3 bonding, broken sp^2 bonds in the sidewalls) in the MWCNTs and G-band is attributed to sp^2 graphitic nature of the MWCNTs[40,48].
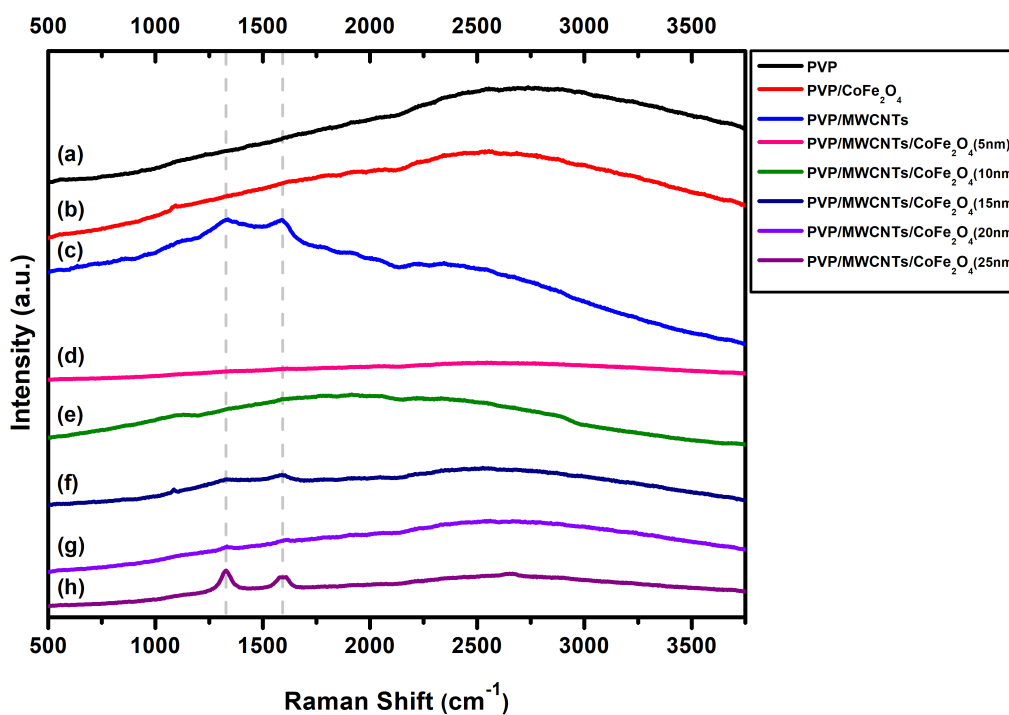
Figure 4.6: Raman spectra of fibers of PVP, PVP/CoFe$_2$O$_4$, PVP/MWCNT and PVP/MWCNT/CoFe$_2$O$_4$.

Figure 4.7 was used to study the interactions between $CoFe_2O_4$ nanoparticles(5,10,15,20,25nm), carbon nanotubes and PVP polymer. The PVP/CNT/$CoFe_2O_4$(5,10,15,20,25nm) spectra exhibit 2 well defined peaks at 1329 and 1590 cm^{-1} corresponding to D-band and G-band, respectively as can see in the table 4.1. Moreover, the position of these peaks remains in the same position as the PVP/MWCNTs spectrum (Fig.4.6).
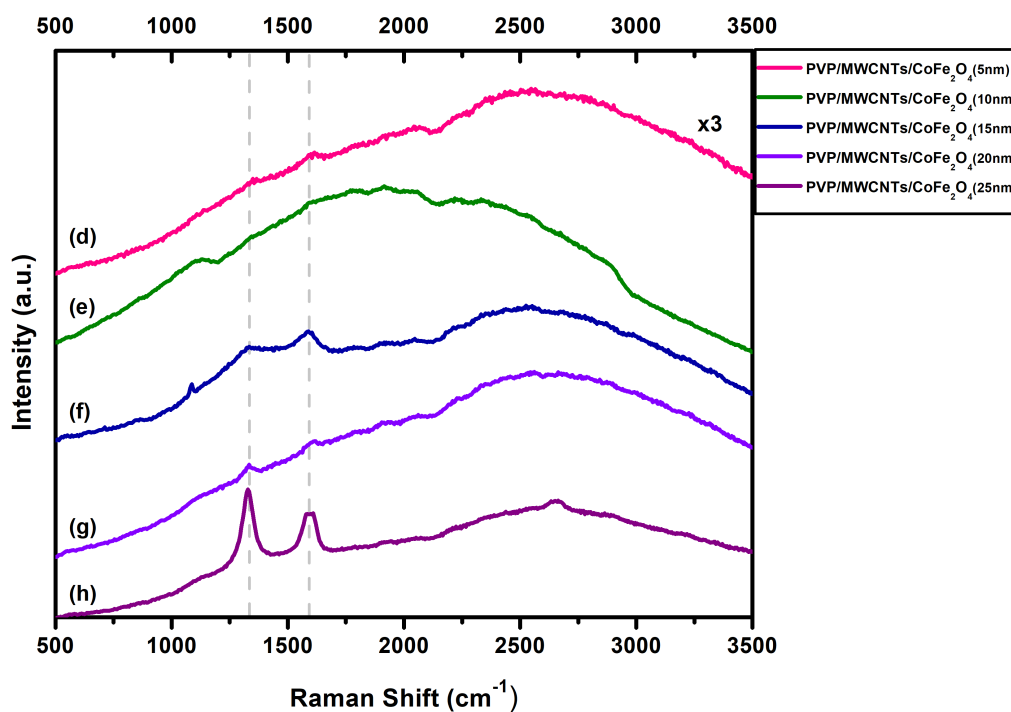
Figure 4.7: Zoom of Raman spectra of PVP/MWCNT/ $CoFe_2O_4$ fibers.

Sample	G-mode	D-mode
(fibers)	(cm^{-1})	(cm^{-1})
PVP/MWCNT	1329	1590
PVP/MWCNT/$CoFe_2O_4$ (5nm)	1329	1590
PVP/MWCNT/$CoFe_2O_4$(10nm)	1329	1590
PVP/MWCNT/$CoFe_2O_4$(15nm)	1329	1590
PVP/MWCNT/$CoFe_2O_4$(20nm)	1329	1590
PVP/MWCNT/$CoFe_2O_4$(25nm)	1329	1590

Table 4.1: Raman vibrational peaks of PVP/MWCNT/ $CoFe_2O_4$ fibers.

4.2.3   Fourier Transform Infrared Spectroscopy (FTIR)

Figure 4.8 shows the FTIR spectra of PVP fibers, PVP/$CoFe_2O_4$ fibers, PVP/MWCNT fibers, PVP/MWCNT/ $CoFe_2O_4$ fibers, $CoFe_2O_4$ nanoparticles and carbon nanotubes. The FTIR spectrum wavenumber ranged from 4000 cm^{-1} to 500 cm^{-1}. The FTIR spectrum of PVP: The O-H stretching vibration of water molecules is observed at 3337 cm^{-1}, which is in the range of 3000-3700 cm^{-1}[49]. It means that PVP nanofibers absorbed water molecules of the air because PVP is hydrophilic[49]. Subsequently, the peak 2972 cm^{-1} is attributed to CH tensile band, while that at 1663 cm^{-1} corresponding to C=O tensile band ($\sim$ 1664 cm^{-1})[44]. Then, CH_2 flexural band is represented by the peak at 1378 cm^{-1} and C-N tensile band by the peak at 1291 cm^{-1} ($\sim$ 1290 cm^{-1})[49].

The FTIR spectra of PVP/$CoFe_2O_4$, PVP/MWCNT, PVP/CNT/$CoFe_2O_4$ have the same peak positions of PVP as can see in the table4.2. It is due to the concentration of CNT and $CoFe_2O_4$ nanoparticles being lower than PVP polymer, making that PVP spectrum overlap the peaks of CNT and $CoFe_2O_4$ nanoparticles.

The FTIR spectrum of $CoFe_2O_4$ nanoparticles: O-H streching vibration is observed at 3250 cm^{-1}, and C=O tensile band at 1542 cm^{-1} due to absorbed water on the surface of the synthesis[50]. Furthermore, the CH tensile band appears at 2914 cm^{-1}, which is in the range of 2850-2931 cm^{-1}[51]. This peak is due to oleic acid used in $CoFe_2O_4$ nanoparticles synthesis[52]. Additionally, the peak at 576 cm^{-1} is identified as Co-O stretching corresponding to vibrations of the metals (octahedral and tetrahedral sites) of the cobalt ferrite[50,52].

The FTIR spectrum of MWCNTs shows a characteristic peak at 3248 cm^{-1} corresponding to tensile band O-H. Band associated to water[35]. Moreover, vibrational mode C=O of the carboxyl functional groups

(-COOH) is observed at 1700 cm^{-1}, which is in the range of 1750–1550 cm^{-1} [35]. The peak ~1640 cm^{-1} is associated with the C=C stretch of the MWCNTs [53] while the peak 1547 cm^{-1} is associated with vibrational mode C-O [54].
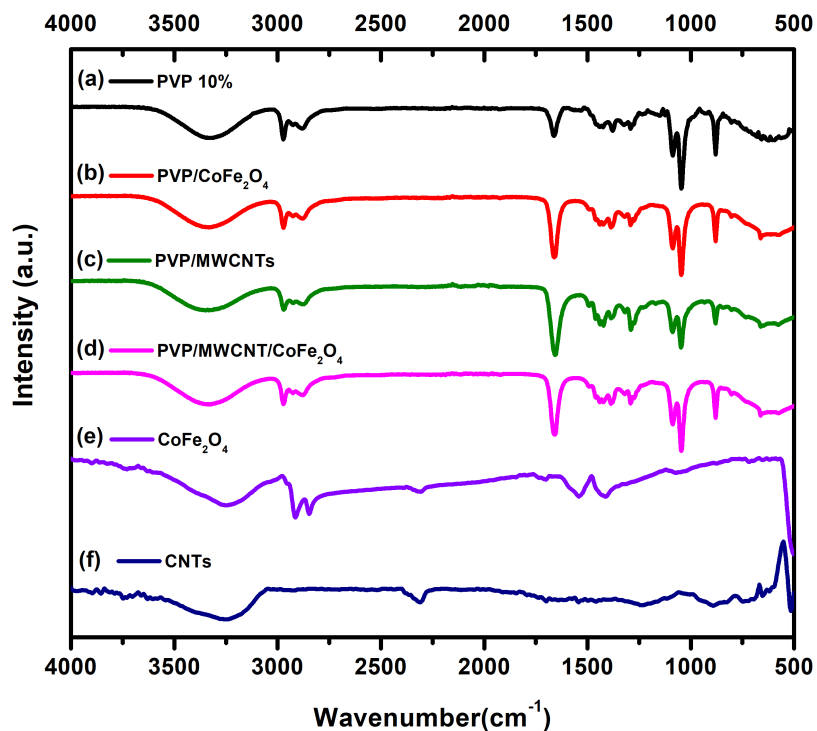
Figure 4.8: FTIR spectra of PVP (black), PVP/CoFe$_2$O$_4$ (red), PVP/MWCNT (green), PVP/MWCNT/CoFe$_2$O$_4$ (magenta) fibers, CoFe$_2$O$_4$ nanoparticles (purple) and carbon nanotubes (blue).

PVP	PVP/ $CoFe_2O_4$	PVP/MWCNT	PVP/MWCNT/ $CoFe_2O_4$	$CoFe_2O_4$	MWCNT	Assignment
			FTIR wavenumber			
			cm^{-1}			
3337	3337	3337	3337	3250	3272	O–H stretch
2972	2972	2972	2972	2914	-	C-H stretch
1663	1663	1663	1663	1542	1700	C=O stretch
-	-	-	-	-	1640	C=C stretch
-	-	-	-	-	1547	C-O stretch
1378	1378	1378	1378	-	-	CH_2 stretch
1291	1291	1291	1291	-	-	C-N stretch
-	-	-	-	576	-	Co-O stretch

Table 4.2: FTIR wavenumber of fibers of PVP, PVP/ $CoFe_2O_4$, PVP/MWCNT, PVP/MWCNT/ $CoFe_2O_4$, $CoFe_2O_4$ nanoparticles and MWCNT.

4.2.4 Thermogavimetric Analysis (TGA)

Figure 4.9, shows the thermograms of the fibers of PVP, PVP/$CoFe_2O_4$, PVP/MWCNT and PVP/MWCNT/$CoFe_2O_4$. The first decrease below 100^oC corresponds to water/ethanol in these thermograms. Then, the pure PVP fibers have a second state thermal decomposition starting at 410^oC and completely decompose at 451^oC. The second thermal decomposition of PVP/$CoFe_2O_4$ fibers starts to 407^oC and fibers are completely decomposed at 460^oC. The PVP/MWCNTs and PVP/MWCNT/$CoFe_2O_4$ fibers have a second decrease from 407^oC to 448^oC and 408^oC to 450^oC, respectively. There is no evidence of a clear change in thermal decomposition material due to the low concentrations of MWCNT, $CoFe_2O_4$, and MWCNT/$CoFe_2O_4$ into the polymer matrix.
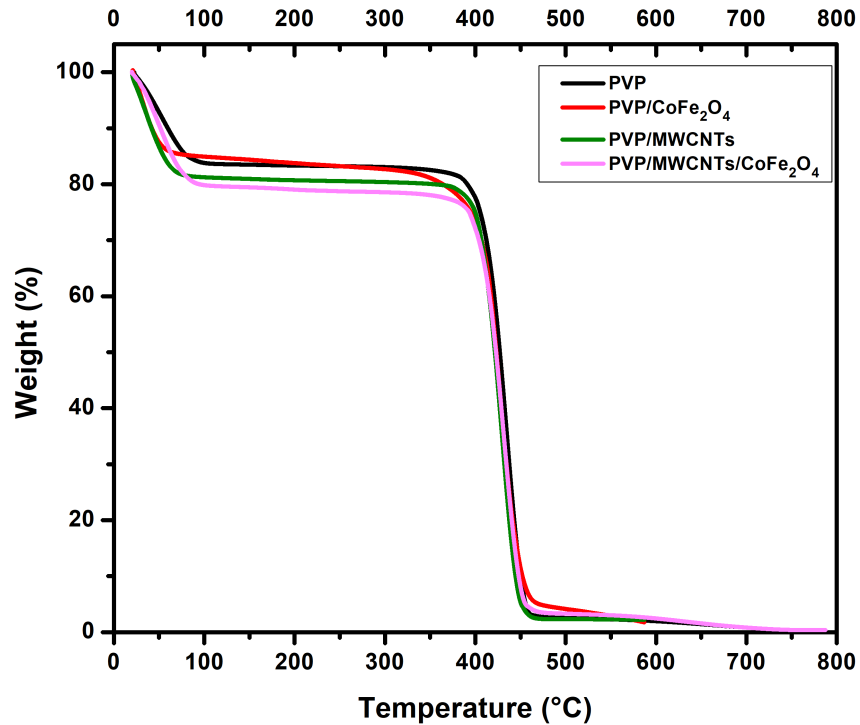
Figure 4.9: Thermograms of PVP, PVP/CoFe$_2$O$_4$, PVP/MWCNT and PVP/MWCNT/CoFe$_2$O$_4$.

4.3   Voltage vs Resistance

Once the fibers of PVP and the composites were obtained and deposited on interdigitated circuits, their electrical properties were analyzed. The PVP and composite fibers were characterized with a DC voltage from 421 to 100 V. Table 4.3 indicates an analysis of pure PVP fibers, achieving a resistance of 52.6 GΩ with an applied voltage of 421 V. Furthermore, it is clear that when the applied voltage is reduced, the resistance of fibers increases. An linear tendency is observed in the voltage against resistance measurements (Fig. 4.10)

The PVP/CoFe$_2$O$_4$(5nm) fibers exhibit a decrement in the resistance against PVP fibers (Table 4.4), obtaining a resistance of 4.70 GΩ with an applied voltage of 420 V. Moreover, figure 4.11 shows a linear tendency of voltage vs. resistance where the applied voltage is inversely proportional to the resistance

of composite fibers. The PVP/CoFe$_2$O$_4$(10 nm) fibers achieve a resistance of 3.81 GΩ with an applied voltage of 421 V. It is evident that all measurements have lower resistance values than PVP fibers. In the same way, the resistance is inversely proportional to the applied voltage with a linear tendency (Fig. 4.12). The PVP/CoFe$_2$O$_4$(15 nm) fibers have a resistance of 5.3 GΩ with an applied voltage of 421 V (Table 4.6). As can be seen in the figure 4.13, there is an exponential tendency where the resistance increases when the applied voltage decreases. The electrons do not flow easily with an applied low voltage. In the case of PVP/CoFe$_2$,O$_4$(20 nm) fibers exhibit a linear tendency where the resistance increases when the applied voltage decreases (Fig.4.14). These composite fibers got a resistance value of 0.99 GΩ with an applied voltage of 421 V, achieving the best results in these composite fibers as seen in the figure 4.22. It means that the electrons flow more easily into the polymer matrix. The PVP/CoFe$_2$O$_4$(25 nm) has a resistance of 5.2 GΩ with an applied voltage of 421 V. This sample shows a resistance linear tendency with applied high voltage values, but the resistance has an exponential increment while applied voltage decreases. As can seen, the composite fibers of PVP/CoFe$_2$O$_4$(5,10,15,20, and 25 nm) exhibit a resistance reduction from around 4 to 50 times in comparison to PVP fibers. Lanus et al. (2020)[55] reported that adding CoFe$_2$O$_4$ nanoparticles to poly (3, 4-ethylenedioxythiophene) improves the electrical conductivity of polymer.

The PVP/MWCNTs fibers obtained a resistance value of 5.25 GΩ with an applied voltage of 421 V (Table 4.9). This value is 10 times less than the resistance of PVP fibers (Fig.4.22). It means that the contribution of MWCNTs to the polymer matrix improved the electrical properties, making electrons flow more easily into the composite fibers. It agrees with Nasouri et al. (2016)[10], who reported that the electrical conductivity of PVP fibers improved when MWCNTs were added to an an electrospinning solution. It means that PVP/MWCNTs composite nanofibers presented lower resistance than PVP fibers. Additionally, the figure 4.16 shows an exponential tendency where the resistance decreases when the applied voltage increases.

The PVP/MWCNTs/CoFe$_2$O$_4$(5 nm) presents a resistance of 14.51 GΩ using an applied voltage of 421 V. Additionally, when the applied voltage decreases, the resistance increases, as can seen in the table4.10. The voltage as a function of resistance measurements show an exponential tendency where the resistance is inversely proportional to applied voltage (Fig.4.17). The PVP/MWCNTs/CoFe$_2$O$_4$(10 nm) exhibits an exponential tendency between voltage and resistance. This behavior is similar to PVP/MWCNTs/CoFe$_2$O$_4$(15 nm), and PVP/MWCNTs/CoFe$_2$O$_4$(20 nm) due to electrons cannot flow easily, producing high resistance values. In these cases, the resistance has a linear tendency with high voltages, but when the applied voltage decreases until 100 V, the resistance increases exponentially. The PVP/MWCNTs/CoFe$_2$O$_4$(25 nm) has the same behavior as their previous composites fibers, but the resistance values are lower than PVP/MWCNTs/CoFe$_2$O$_4$(5,10,15 and 20nm). Therefore, PVP/MWCNTs/CoFe$_2$O$_4$(5,10,15,20,25nm)

composite fibers achieved lower resistance values than PVP fibers. Alghamdi et al. (2022)[56] created CMC/PVA nanocomposites doped with $CoFe_2O_4$/MWCNTs where the energy gap of nanocomposite films decreased when $CoFe_2O_4$/MWCNTs were added to the polymer. It means that the electrical properties of $CoFe_2O_4$ and MWCNTs help so that electrons travel more easily through the composite structure of fibers.

PVP fibers			
Input Voltage (V_o)	**Output Voltage (V_f)**	**Resistance (R_X)**	**Interdigitated Voltage (V_X)**
V	V	GΩ	V
421	0.08	52.61	420.91
355	0.04	88.74	354.96
290	0.02	144.99	289.98
200	0.01	199.99	199.99
100	0.00	-	-

Table 4.3: Voltage vs resistance results of PVP fibers.
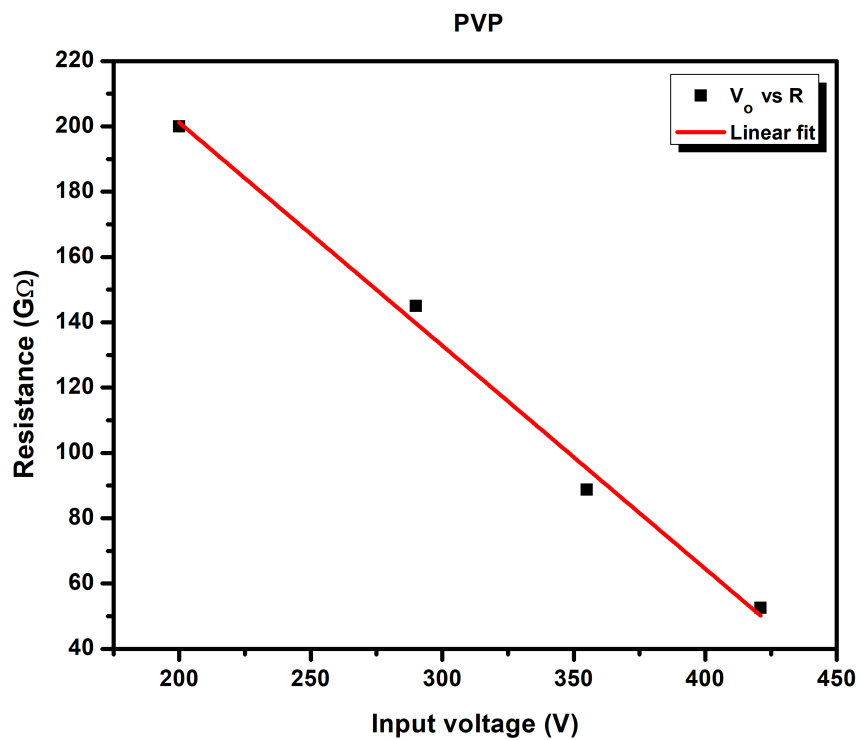
Figure 4.10: Voltage vs resistance results of PVP fibers.

PVP/CoFe$_2$O$_4$ (5nm) fibers			
Input Voltage (V_o)	Output Voltage (V_f)	Resistance (R_X)	Interdigitated Voltage (V_X)
V	V	GΩ	V
420	0.89	4.71	419.01
354	0.71	4.97	353.21
284	0.52	5.45	283.42
209	0.38	5.49	208.58
94	0.15	6.26	93.83

Table 4.4: Voltage vs resistance results of PVP/CoFe$_2$O$_4$ (5nm) fibers.
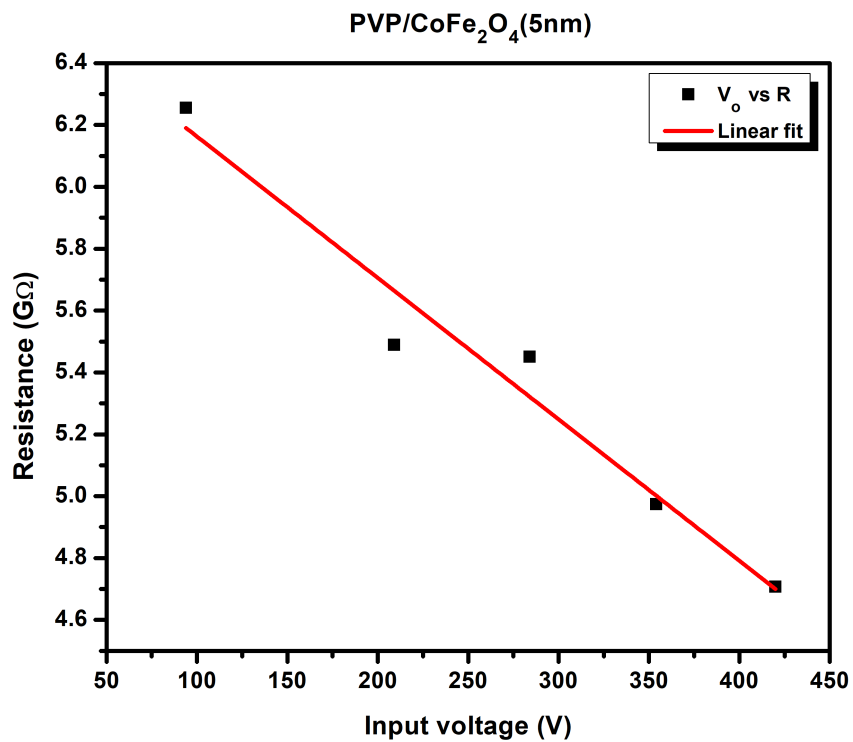
Figure 4.11: Voltage vs resistance results of PVP/CoFe$_2$O$_4$ (5nm) fibers.

PVP/CoFe$_2$O$_4$ (10nm) fibers			
Input Voltage (V$_o$)	**Output Voltage (V$_f$)**	**Resistance (R$_X$)**	**Interdigitated Voltage (V$_X$)**
V	V	GΩ	V
421	1.10	3.82	419.77
367	0.90	4.07	365.99
290	0.70	4.13	289.22
200	0.48	4.16	199.46
100	0.22	4.53	99.75

Table 4.5: Voltage vs resistance results of PVP/CoFe$_2$O$_4$ (10nm) fibers.
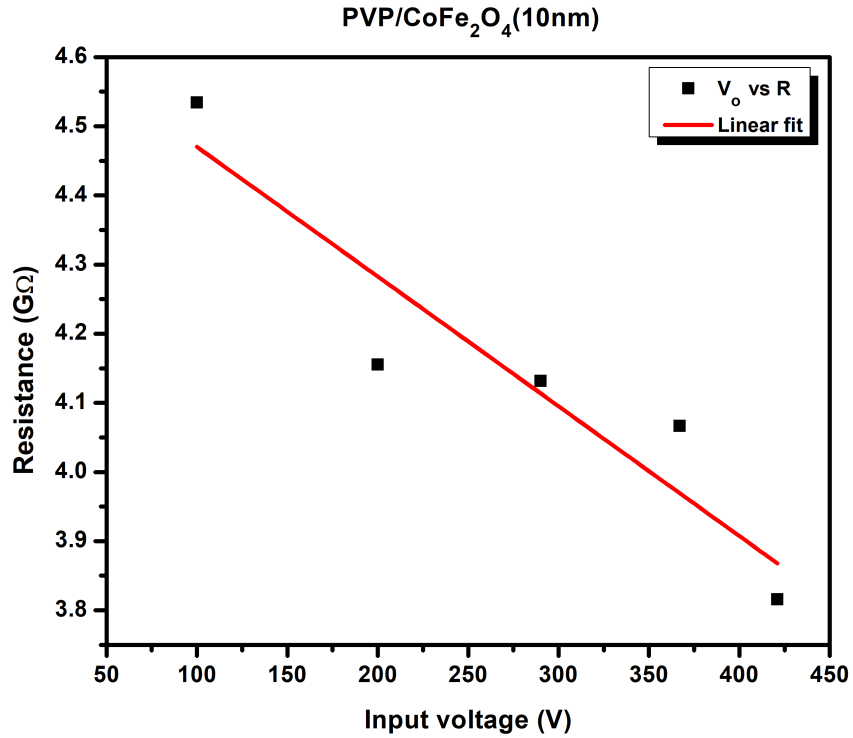
Figure 4.12: Voltage vs resistance results of PVP/CoFe$_2$O$_4$ (10nm) fibers

PVP/CoFe$_2$O$_4$ (15nm) fibers			
Input Voltage (V_o) V	**Output Voltage (V_f)** V	**Resistance (R_X)** GΩ	**Interdigitated Voltage (V_X)** V
421	0.79	5.32	420.12
355	0.66	5.37	354.26
290	0.50	5.79	289.44
200	0.34	5.87	199.62
100	0.14	7.13	99.84

Table 4.6: Voltage vs resistance results of PVP/CoFe$_2$O$_4$ (15nm) fibers.
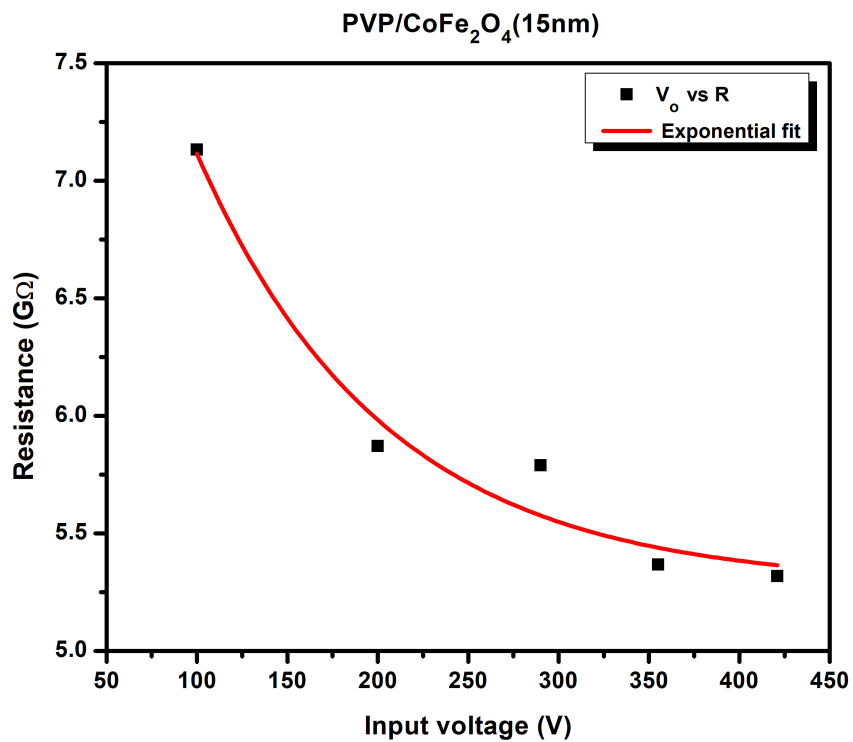
Figure 4.13: Voltage vs resistance results of PVP/CoFe$_2$O$_4$ (15nm) fibers

PVP/CoFe$_2$O$_4$ (20nm) fibers			
Input Voltage (V$_o$) V	**Output Voltage (V$_f$)** V	**Resistance (R$_X$)** GΩ	**Interdigitated Voltage (V$_X$)** V
421	4.20	0.99	416.30
355	3.39	1.04	351.21
290	2.42	1.19	287.29
200	1.50	1.32	198.32
100	0.67	1.48	99.25

Table 4.7: Voltage vs resistance results of PVP/CoFe$_2$O$_4$ (20nm) fibers.
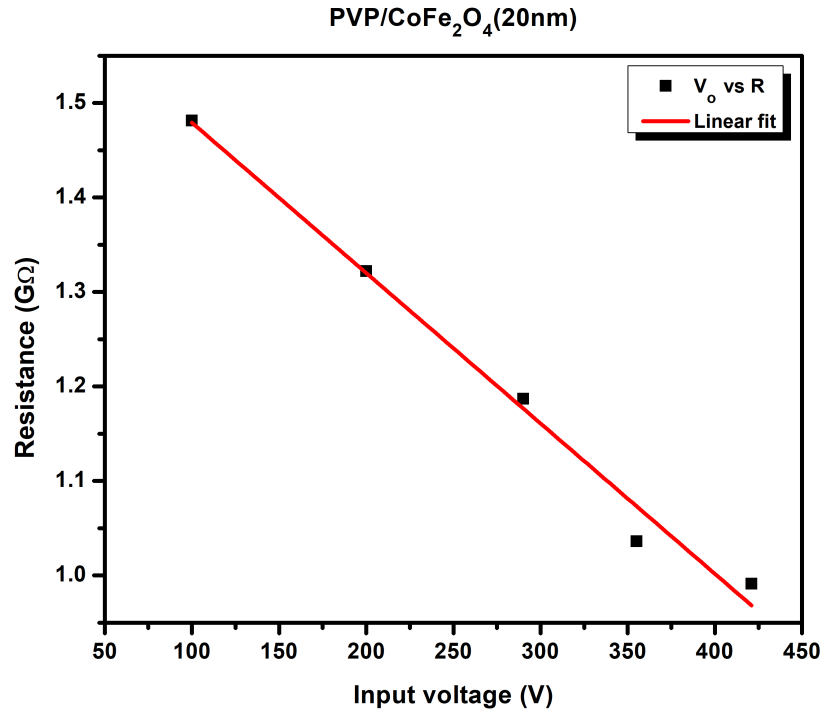
Figure 4.14: Voltage vs resistance results of PVP/CoFe$_2$O$_4$ (20nm) fibers

PVP/CoFe$_2$O$_4$ (25nm) fibers			
Input Voltage (V$_o$) V	**Output Voltage (V$_f$)** V	**Resistance (R$_X$)** GΩ	**Interdigitated Voltage (V$_X$)** V
420	0.90	4.67	419.99
355	0.75	4.72	354.16
290	0.61	4.74	289.32
200	0.33	6.05	199.63
100	0.15	6.66	99.83

Table 4.8: Voltage vs resistance results of PVP/CoFe$_2$O$_4$ (25nm) fibers.
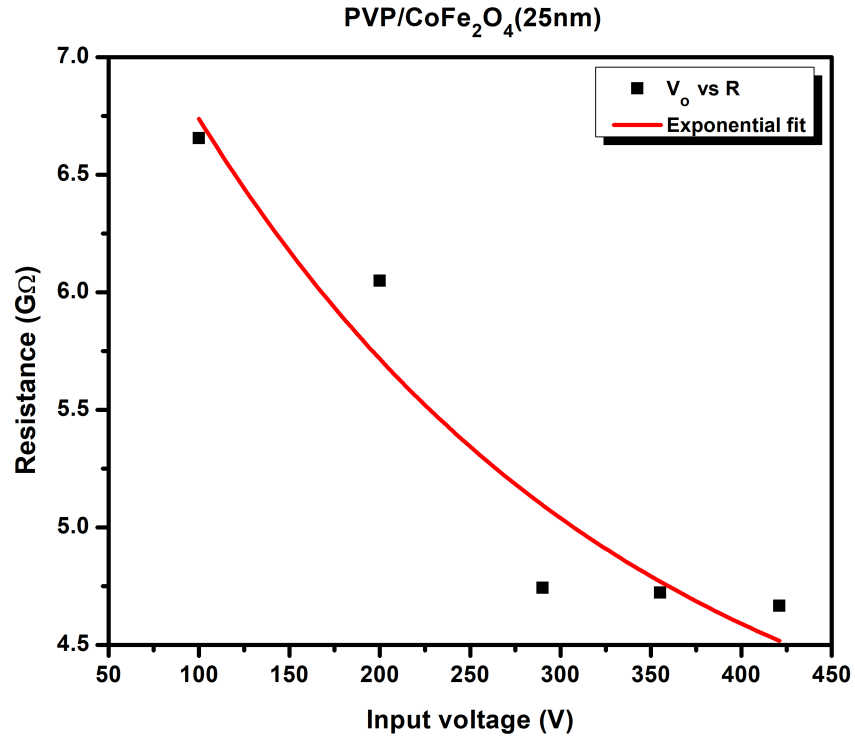
Figure 4.15: Voltage vs resistance results of PVP/CoFe$_2$O$_4$ (25nm) fibers

PVP/MWCNTs fibers			
Input Voltage (V$_o$)	**Output Voltage (V$_f$)**	**Resistance (R$_X$)**	**Interdigitated Voltage (V$_X$)**
V	V	GΩ	V
421	0.80	5.25	420.11
355	0.65	5.45	354.27
290	0.52	5.57	289.41
200	0.35	5.70	199.61
100	0.16	6.24	99.82

Table 4.9: Voltage vs resistance results of PVP/MWCNTs fibers
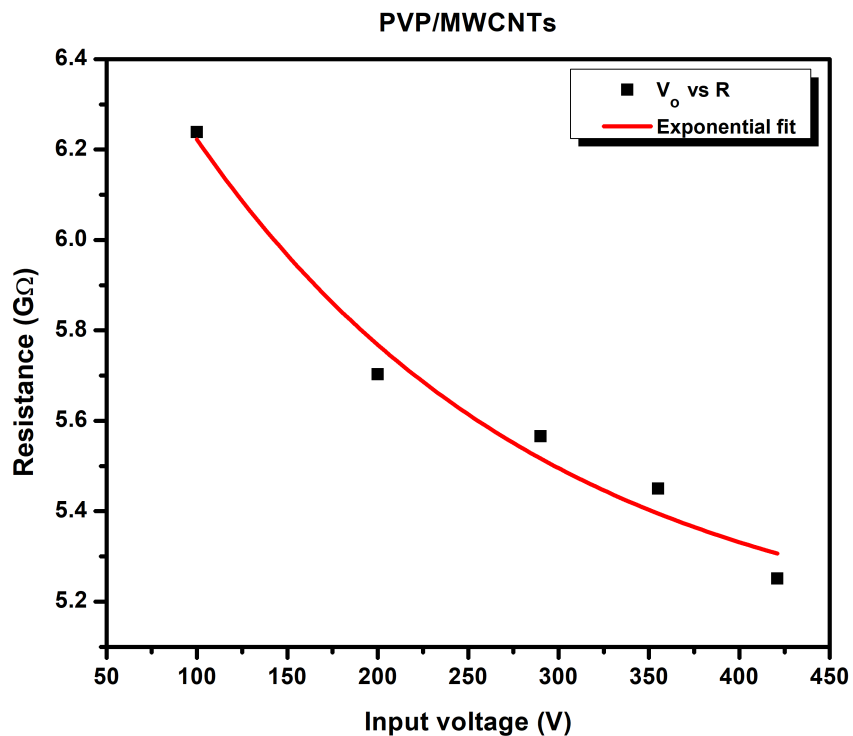
Figure 4.16: Voltage vs resistance results of PVP/MWCNTs fibers

PVP/MWCNTs/CoFe$_2$O$_4$(5nm) fibers			
Input Voltage (V_o) V	Output Voltage (V_f) V	Resistance (R_X) GΩ	Interdigitated Voltage (V_X) V
421	0.29	14.51	420.68
357	0.24	14.86	356.74
290	0.19	15.25	289.80
200	0.13	15.37	199.87
100	0.06	16.66	99.94

Table 4.10: Voltage vs resistance results of PVP/MWCNT/CoFe$_2$O$_4$ (5nm) fibers
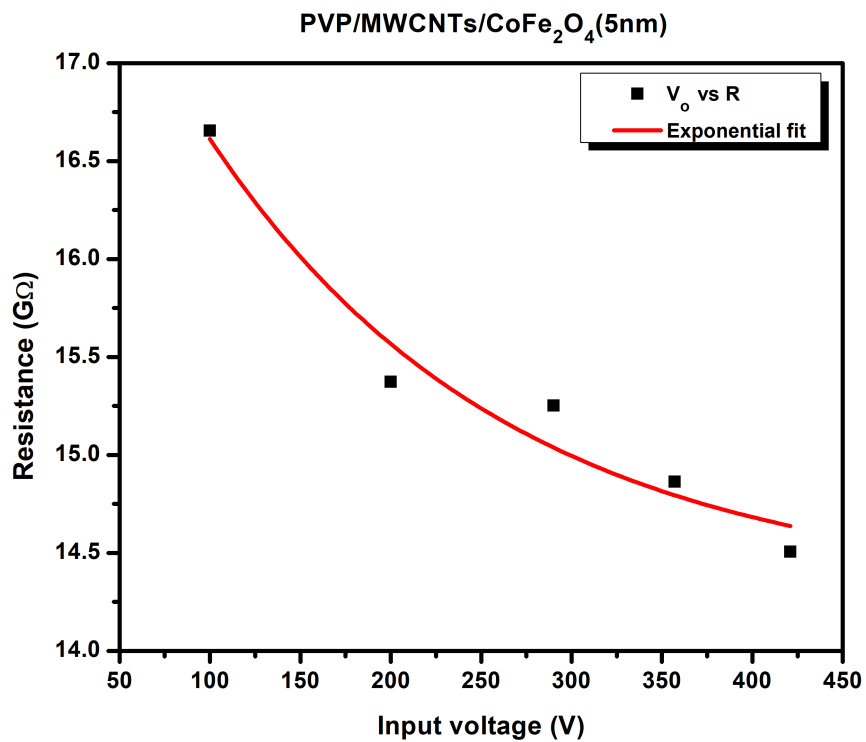
Figure 4.17: Voltage vs resistance results of PVP/MWCNT/CoFe$_2$O$_4$ (5nm) fibers

PVP/MWCNTs/CoFe$_2$O$_4$(10nm) fibers			
Input Voltage (V_o)	**Output Voltage (V_f)**	**Resistance (R_X)**	**Interdigitated Voltage (V_X)**
V	V	GΩ	V
421	0.19	22.15	420.79
357	0.14	25.35	354.84
290	0.06	48.32	289.93
200	0.03	66.66	199.97
100	0.01	99.99	99.99

Table 4.11: Voltage vs resistance results of PVP/MWCNT/CoFe$_2$O$_4$ (10nm) fibers
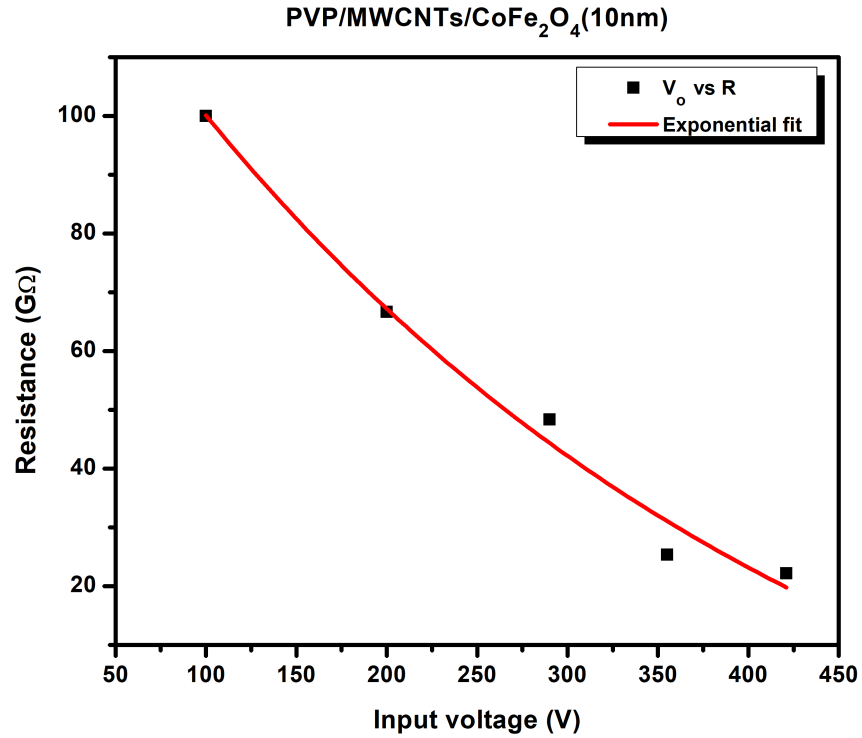
Figure 4.18: Voltage vs resistance results of PVP/MWCNT/CoFe$_2$O$_4$ (10nm) fibers

PVP/MWCNTs/CoFe$_2$O$_4$(15nm) fibers			
Input Voltage (V_o) V	**Output Voltage (V_f)** V	**Resistance (R_X)** GΩ	**Interdigitated Voltage (V_X)** V
420	0.21	19.99	419.77
355	0.17	20.87	354.81
290	0.13	22.30	289.86
200	0.08	24.99	199.91
100	0.03	33.32	99.67

Table 4.12: Voltage vs resistance results of PVP/MWCNT/CoFe$_2$O$_4$ (15nm) fibers
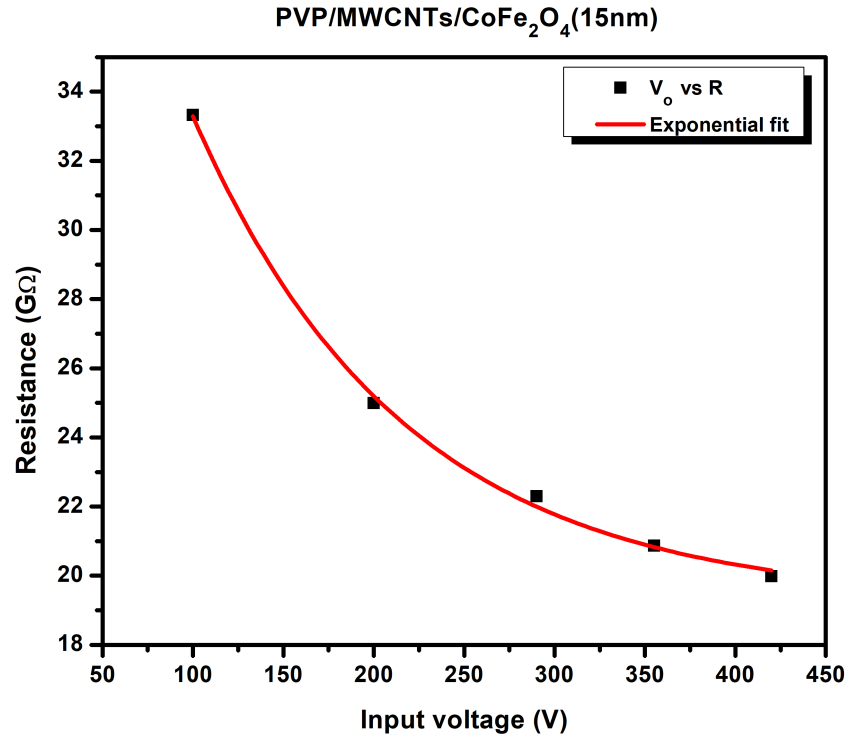
Figure 4.19: Voltage vs resistance results of PVP/MWCNT/CoFe$_2$O$_4$ (15nm) fibers

PVP/MWCNTs/CoFe$_2$O$_4$(20nm) fibers			
Input Voltage (V_o)	**Output Voltage (V_f)**	**Resistance (R_X)**	**Interdigitated Voltage (V_X)**
V	V	GΩ	V
420	0.18	23.32	419.78
355	0.15	23.66	354.83
290	0.12	24.16	289.87
200	0.08	24.99	199.91
100	0.03	33.32	99.97

Table 4.13: Voltage vs resistance results of PVP/MWCNT/CoFe$_2$O$_4$ (20nm) fibers
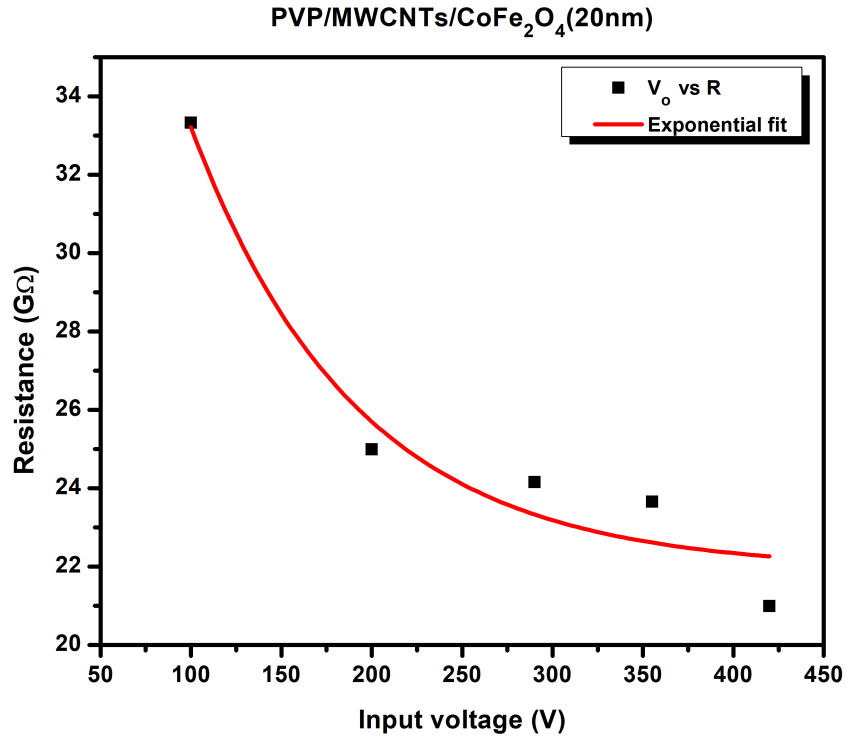
Figure 4.20: Voltage vs resistance results of PVP/MWCNT/CoFe$_2$O$_4$ (20nm) fibers

PVP/MWCNTs/CoFe$_2$O$_4$(25nm) fibers			
Input Voltage (V$_o$)	**Output Voltage (V$_f$)**	**Resistance (R$_X$)**	**Interdigitated Voltage (V$_X$)**
V	V	GΩ	V
421	0.30	14.02	420.67
357	0.24	14.78	354.73
290	0.19	15.25	289.79
200	0.12	16.66	199.87
100	0.05	19.99	99.94

Table 4.14: Voltage vs resistance results of PVP/MWCNT/CoFe$_2$O$_4$ (25nm) fibers
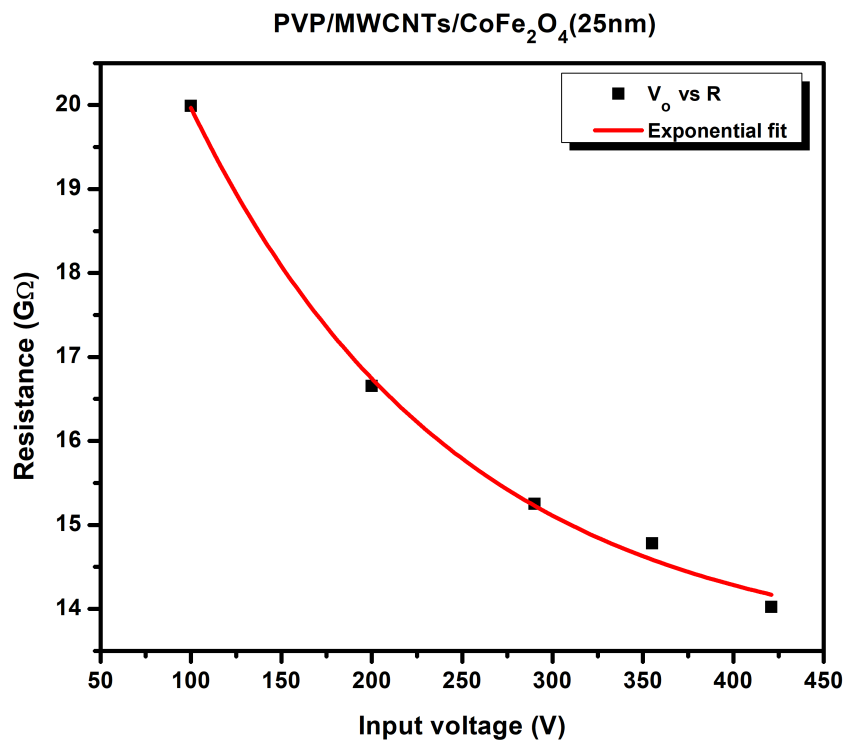
Figure 4.21: Voltage vs resistance results of PVP/MWCNT/CoFe$_2$O$_4$ (25nm) fibers

Figure 4.22 shows a semi-log comparative graph of resistance values at high and low voltages. It is important to consider the samples as four classifications: a) PVP, b) PVP/CoFe$_2$O$_4$ c) PVP/MWCNTs, and d) PVP/MWCNTs/CoFe$_2$O$_4$. Firstly, pure PVP fibers exhibit the highest resistance value at ~420 V. Nevertheless, it was not possible to calculate the resistance value at ~100V due to electrons not flowing through the polymer matrix. Secondly, PVP/CoFe$_2$O$_4$ (5,10,15,20,25nm) fibers show resistance values from 0.99 to 5.31 GΩ and from 1.48 to 7.13 GΩ at ~420 and ~100 V, respectively. It is clear that PVP/CoFe$_2$O$_4$ (20nm) had the lowest resistance of all samples at high and low voltages. Thirdly, PVP/MWCNTs also reduced resistance against the PVP fibers at high and low voltages. Finally, PVP/MWCNTs/CoFe$_2$O$_4$ (5,10,15,20,25 nm) also exhibited a reduction of resistance but obtained the highest resistances of all composites.
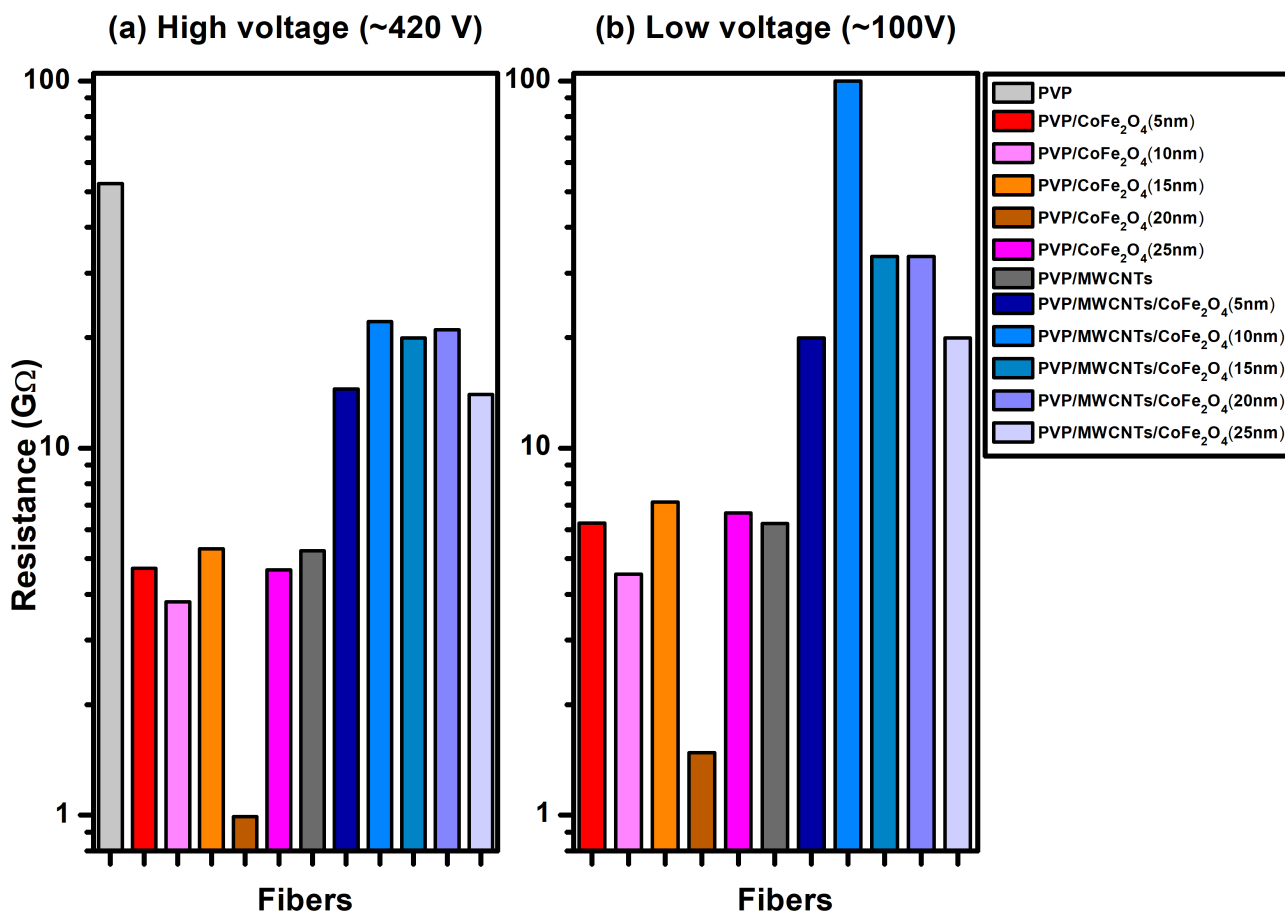
Figure 4.22: A semi log comparative graph of resistance values at a) high and b) low applied voltages.

To sum up, an average analysis of voltage against the resistance was done, as seen in the table 4.15.

Fibers	Applied voltage (V)	Output voltage (V)	Resistance (GΩ)
PVP	316.5	0.0375	121.58
PVP/CoFe$_2$O$_4$(5nm)	272.2	0.530	5.38
PVP/CoFe$_2$O$_4$(10nm)	275.6	0.68	4.14
PVP/CoFe$_2$O$_4$(15nm)	273.2	0.486	5.90
PVP/CoFe$_2$O$_4$(20nm)	273.2	1.5925	1.20
PVP/CoFe$_2$O$_4$(25nm)	273.2	0.548	5.37
PVP/MWCNTs	273.2	0.496	5.64
PVP/MWCNTs/CoFe$_2$O$_4$(5nm)	273.6	0.182	15.33
PVP/MWCNTs/CoFe$_2$O$_4$(10nm)	273.2	0.086	52.49
PVP/MWCNTs/CoFe$_2$O$_4$(15nm)	273	0.124	24.29
PVP/MWCNTs/CoFe$_2$O$_4$(20nm)	273	0.112	25.89
PVP/MWCNTs/CoFe$_2$O$_4$(25nm)	273.2	0.18	16.14

Table 4.15: Average applied voltage, output voltage and resistance values
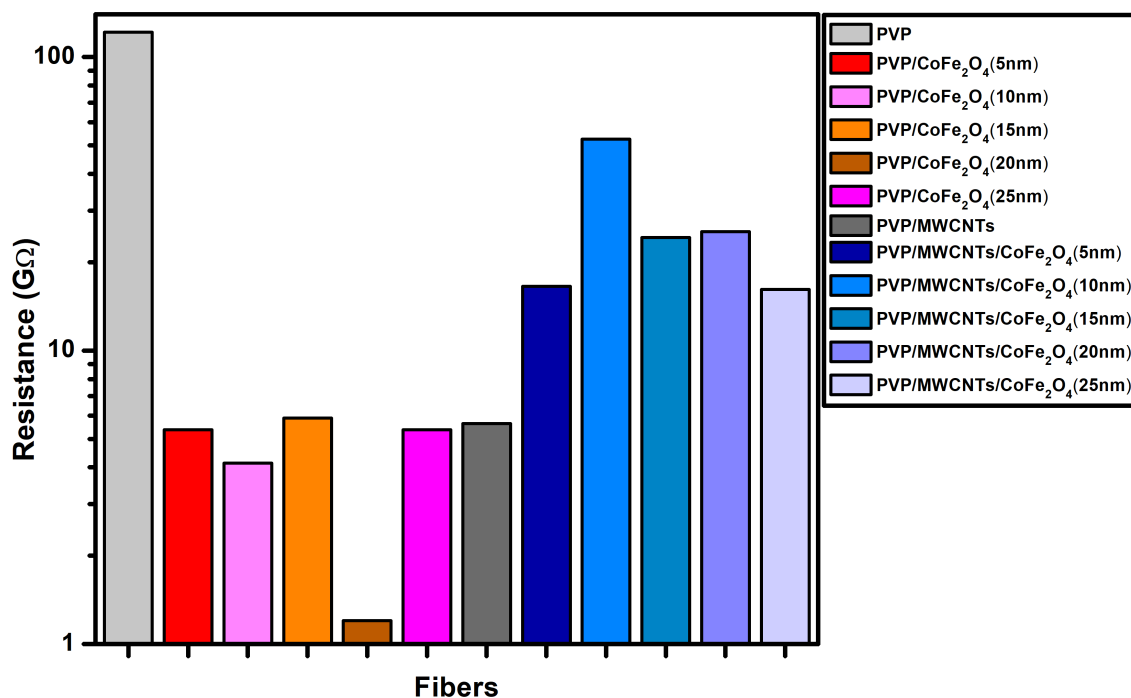
Figure 4.23: A semi log graph of average resistance values.

Figure 4.23 shows that the PVP fibers have the highest resistance value due to the insulating properties of the material, making electrons cannot flow easily between the insulator matrix[10]. PVP fibers obtained were smooth and free from beads (Fig. 4.3a) because the collecting distance parameter was optimum in the electrospinning process as reported in the literature[24].

PVP/$CoFe_2O_4$(5,10,15,20,25nm) fibers present a resistance reduction by two orders of magnitude (Tab.4.15). It agrees with Lanus et al. (2020), who reported that adding $CoFe_2O_4$ nanoparticles to polymer improves the electrical conductivity[55]. Nevertheless, a good dispersion of $CoFe_2O_4$ nanoparticles into the PVP solution was not obtained. It is evident because the figures 4.3b,4.3c,4.3d, 4.3e and 4.3f present droplets between the fibers where the size of droplets increased against the size of the nanoparticles. This effect occurs because the magnetic nanoparticles tend to agglomerate due to their large surface energy and

strong magnetic interactions[57]. Therefore, when the size of nanoparticles increases, the surface energy and magnetic interaction increases, too, producing an increment of droplet sizes. However, if the droplets do not affect the fiber's formation, they appear as islands, helping to flow of electrons. In fact, if the amount of islands is high, the electrical conductivity would increase because electron transport in composite usually occurs between nearest-neighbor particles at close proximity[58]. It is because $PVP/CoFe_2O_4$(20nm) fibers obtained the lowest resistance value. Nevertheless, FTIR and Raman spectra indicated that $CoFe_2O_4$ vibrational modes were overlapped by the PVP spectrum due to low concentration of nanoparticles in polymer matrix (Fig. 4.6,4.8).

The PVP/MWCNTs and $PVP/MWCNTs/CoFe_2O_4$ fibers also exhibit a resistance reduction against the PVP fibers in which $CoFe_2O_4$ and CNTs provided electrical conduction to polymer matrix[58]. Nevertheless, the literature reported that PVP/MWCNTs and $PVP/MWCNTs/CoFe_2O_4$ have the highest conductivity than $PVP/CoFe_2O_4$ in solution/suspension. It could be affected by the dispersion of nanomaterials into polymer solutions. $PVP/CoFe_2O_4$, PVP/MWCNTs, and $PVP/MWCNTs/CoFe_2O_4$ were sonicated at 3min 50 s, 4 min 30 s, and from 3 to 4 min, respectively. The time difference between them is very close, which would produce agglomerations of MWCNTs in PVP/MWCNTs and $PVP/MWCNTs/CoFe_2O_4$. It is known that when MWCNTs tend to agglomerate due to dispersion and interfacial interactions, they do not allow the formation of conductive pathways[58], increasing the resistance of composites (Fig.4.23). Furthermore, FTIR spectra exhibited an overlap of MWCNTs and $CoFe_2O_4$ vibrational modes by PVP due to low concentration of these nanomaterials (Fig.4.8). Raman spectra show the vibrational bands (D-band, G-band) of MWCNTs in composite fibers.

The last composite obtained the worst resistance results by analyzing the resistance values of PVP/MWCNTs and $PVP/MWCNTs/CoFe_2O_4$. It would be affected by dispersion time and concentration of MWCNTs and it is observed in the composite intensities of Raman spectra (Fig.4.6,4.7) Finally, low concentration of nanoparticles and MWCNTs into PVP solution made that TGA thermogram does not exhibit major changes between them (Fig.4.9).

Chapter 5

Conclusions & Outlook

The present work reported the fabrication of PVP, PVP/ $CoFe_2O_4$ (5,10,15,20,25 nm), PVP/MWCNT, and PVP/MWCNT/$CoFe_2O_4$ (5,10,15,20,25 nm) fibers by electrospinning technique, obtaining an average diameter of 4.13μm, 1.90μm, 2.11μm and 0.78μm, respectively. To find the optimum parameters for obtaining fibers, 20 electrospinning trials were conducted. The fabricated fibers were characterized by optical microscopy, TGA, Raman, and FTIR to observe their structure and composition. Electrical properties were characterized using a homemade electrical device. The voltage against the resistance analysis showed that the resistance of PVP and the composite fibers reduces when the applied voltage increases. Furthermore, considering an applied voltage of 421V (high voltage), the PVP fibers showed a resistance of 52.61GΩ. Nevertheless, PVP/$CoFe_2O_4$ (5,10,15,20,25 nm) composite fibers showed a resistance from 0.99 GΩ to 5.31 GΩ. It indicates that adding cobalt-ferrite nanoparticles into a polymeric matrix helps electrons flow. PVP/$CoFe_2O_4$(20nm) shows a resistance reduction of 50 times against the PVP fibers. PVP/MWCNTs fibers exhibited a resistance reduction of 5.2513 GΩ. This value is around 10 times less than PVP fibers. Additionally, it was necessary to observe the effect of multi-walled carbon nanotubes and cobalt-ferrite nanoparticles into a polymeric matrix. PVP/ MWCNTs/$CoFe_2O_4$ (5,10,15,20,25 nm) composite fibers showed a resistance range from 14.02 to 23.32 GΩ. The best result of these composite fibers was from PVP/$CoFe_2O_4$ (25 nm) with a resistance of 14.02 GΩ, maintaining a high applied voltage around 420 V. At low voltage values ∼100 V, the resistance reduction effect of composite fibers concerning pure PVP fibers also was observed. To sum up, voltage as a function of resistance characterization analysis showed that the resistance is inversely proportional to the applied voltage at PVP polymer, and its electrical properties improve when the cobalt ferrite nanoparticles and carbon nanotubes are added.

Bibliography

[1] Kailasa, S.; Reddy, M. S. B.; Maurya, M. R.; Rani, B. G.; Rao, K. V.; Sadasivuni, K. K. Electrospun nanofibers: materials, synthesis parameters, and their role in sensing applications. *Macromolecular Materials and Engineering* **2021**, *306*, 2100410.

[2] Wang, Z.; Wu, S.; Wang, J.; Yu, A.; Wei, G. Carbon nanofiber-based functional nanomaterials for sensor applications. *Nanomaterials* **2019**, *9*, 1045.

[3] Zaarour, B.; Zhu, L.; Jin, X. A review on the secondary surface morphology of electrospun nanofibers: formation mechanisms, characterizations, and applications. *ChemistrySelect* **2020**, *5*, 1335–1348.

[4] Wang, S.-X.; Yap, C. C.; He, J.; Chen, C.; Wong, S. Y.; Li, X. Electrospinning: A facile technique for fabricating functional nanofibers for environmental applications. *Nanotechnology Reviews* **2016**, *5*, 51–73.

[5] Chen, I.-H.; Wang, C.-C.; Chen, C.-Y. Fabrication and characterization of magnetic cobalt ferrite/polyacrylonitrile and cobalt ferrite/carbon nanofibers by electrospinning. *Carbon* **2010**, *48*, 604–611.

[6] Gökmeşe, F.; Uslu, I.; Aytimur, A. Preparation and characterization of PVA/PVP nanofibers as promising materials for wound dressing. *Polymer-Plastics Technology and Engineering* **2013**, *52*, 1259–1265.

[7] Wang, Z.; Wu, S.; Wang, J.; Yu, A.; Wei, G. Carbon nanofiber-based functional nanomaterials for sensor applications. *Nanomaterials* **2019**, *9*, 1045.

[8] Alcalá, O.; Briceño, S.; Brämer-Escamilla, W.; Silva, P. Toroidal cores of MnxCo1- xFe2O4/PAA nanocomposites with potential applications in antennas. *Materials Chemistry and Physics* **2017**, *192*, 17–21.

[9] Shaterian, M.; Aghaei, A.; Koohi, M.; Teymouri, M.; Mohammadi-Ganjgah, A. Synthesis, characterization and electrochemical sensing application of CoFe2O4/graphene magnetic nanocomposite for analysis of atenolol. *Polyhedron* **2020**, *182*, 114479.

[10] Nasouri, K.; Shoushtari, A. M.; Mojtahedi, M. R. M. Theoretical and experimental studies on EMI shielding mechanisms of multi-walled carbon nanotubes reinforced high performance composite nanofibers. *Journal of Polymer Research* **2016**, *23*, 1–8.

[11] Li, X.; Guan, G.; Zhang, K.; Gao, G.; Xiang, J. Flexible CoFe2O4 nanoparticles/N-doped carbon nanofibers membrane as self-standing anode for lithium-ion batteries. *Journal of Alloys and Compounds* **2023**, *946*, 169397.

[12] Burkacky, O.; Dragon, J.; Lehmann, N. The semiconductor decade: A trillion-dollar industry. *McKinsey & Company* **2022**, *1*.

[13] Feynman, R. P. There's plenty of room at the bottom. *Feynman and computation* **2018**, *63*, 76.

[14] Nasrollahzadeh, M.; Sajadi, S. M.; Sajjadi, M.; Issaabadi, Z. *Interface science and technology*; Elsevier, 2019; Vol. 28; pp 1–27.

[15] others,, *et al.* NanoDictionary. *Collegium Basilea, Basel* **2005**,

[16] Corzo, D.; Tostado-Blázquez, G.; Baran, D. Flexible electronics: status, challenges and opportunities. *Frontiers in Electronics* **2020**, *1*, 594003.

[17] others,, *et al.* Magnetic CoFe2O4 nanoparticles doped with metal ions: a review. *Ceramics International* **2020**, *46*, 18391–18412.

[18] Chen, W.; Xia, C.; Alshareef, H. N. One-step electrodeposited nickel cobalt sulfide nanosheet arrays for high-performance asymmetric supercapacitors. *ACS nano* **2014**, *8*, 9531–9541.

[19] Ding, Y.; Ren, C.; Tian, X.; Zhang, M.; Zhang, J.; Sun, K.; Wu, Y.; Sun, H.; Pang, L.; Sha, F. Facile synthesis of aminophenylboronic decorated electrospun CoFe2O4 spinel nanofibers with enhanced electrocatalytic performance for glucose electrochemical sensor application. *Ceramics International* **2021**, *47*, 19052–19062.

[20] Iijima, S. Helical microtubules of graphitic carbon. *nature* **1991**, *354*, 56–58.

[21] Nicholson, J. *The chemistry of polymers*; Royal Society of Chemistry, 2017.

[22] Koczkur, K. M.; Mourdikoudis, S.; Polavarapu, L.; Skrabalak, S. E. Polyvinylpyrrolidone (PVP) in nanoparticle synthesis. *Dalton transactions* **2015**, *44*, 17883–17905.

[23] Su, Z.; Ding, J.; Wei, G. Electrospinning: A facile technique for fabricating polymeric nanofibers doped with carbon nanotubes and metallic nanoparticles for sensor applications. *Rsc Advances* **2014**, *4*, 52598–52610.

[24] Utkarsh,; Hegab, H.; Tariq, M.; Syed, N. A.; Rizvi, G.; Pop-Iliev, R. Towards analysis and optimization of electrospun PVP (polyvinylpyrrolidone) nanofibers. *Advances in Polymer Technology* **2020**, *2020*, 1–9.

[25] Tolouei, N. E.; Ghamari, S.; Shavezipur, M. Development of circuit models for electrochemical impedance spectroscopy (EIS) responses of interdigitated MEMS biochemical sensors. *Journal of Electroanalytical Chemistry* **2020**, *878*, 114598.

[26] Hu, Y.-C.; Dai, C.-L.; Hsu, C.-C. Titanium dioxide nanoparticle humidity microsensors integrated with circuitry on-a-chip. *Sensors* **2014**, *14*, 4177–4188.

[27] Yamamoto, H.; Kato, R.; Miyagawa, K.; Kanoda, K.; Okamoto, H. Mott transition by an impulsive dielectric breakdown. **2017**,

[28] Senthil, T. Theory of a continuous Mott transition in two dimensions. *Physical Review B* **2008**, *78*, 045109.

[29] Davidson, M. W.; Abramowitz, M. Optical microscopy. *Encyclopedia of imaging science and technology* **2002**, *2*, 120.

[30] De Blasio, C.; De Blasio, C. Thermogravimetric analysis (TGA). *Fundamentals of biofuels engineering and technology* **2019**, 91–102.

[31] Elishav, O.; Beilin, V.; Rozent, O.; Shter, G. E.; Grader, G. S. Thermal shrinkage of electrospun PVP nanofibers. *Journal of Polymer Science Part B: Polymer Physics* **2018**, *56*, 248–254.

[32] Nan, D.; Wei, J.; Guo, F.; Fan, G.; Xu, F.; Li, L.; Zhu, H.; Wang, K.; Wu, D. Fabrication and oil adsorption of carbon nanotube/polyvinylpyrrolidone surface composite. *Journal of Nanoscience and Nanotechnology* **2014**, *14*, 6461–6465.

[33] Thomas, S.; Thomas, R.; Zachariah, A. K.; Kumar, R. *Spectroscopic methods for nanomaterials characterization*; Elsevier, 2017; Vol. 2.

[34] Omran, S. M.; Abdullah, E. T.; Al-Zuhairi, O. A. Structural and Infrared Spectroscopy of Polyvinylpyrrolidone/Multi-walled Carbon Nanotubes Nanocomposite. *Iraqi Journal of Physics* **2021**, *19*, 1–6.

[35] Stobinski, L.; Lesiak, B.; Kövér, L.; Tóth, J.; Biniak, S.; Trykowski, G.; Judek, J. Multiwall carbon nanotubes purification and oxidation by nitric acid studied by the FTIR and electron spectroscopy methods. *Journal of alloys and compounds* **2010**, *501*, 77–84.

[36] Urban, M. W. *Fourier transform infrared and Fourier transform Raman spectroscopy of polymers: Principles and applications*; ACS Publications, 1993.

[37] Naumann, A.; Peddireddi, S.; Kües, U.; Polle, A. 10. Fourier Transform Infrared Microscopy in Wood Analysis. *Wood production, wood technology, and biotechnological impacts* **2007**, 179.

[38] Fan, M.; Dai, D.; Huang, B. Fourier transform infrared spectroscopy for natural fibres. *Fourier transform-materials analysis* **2012**, *3*, 45–68.

[39] Smith, E.; Dent, G. *Modern Raman spectroscopy: a practical approach*; John Wiley & Sons, 2019.

[40] Nasouri, K.; Shoushtari, A. M.; Mojtahedi, M. R. M. Synthesis and characterization of highly dispersed multi-walled carbon nanotubes/polyvinylpyrrolidone composite nanofibers for EMI shielding application. *Polymer Composites* **2017**, *38*, 2026–2034.

[41] Wang, J.; Xu, H.; Huo, Y.; Wang, Y.; Dong, M. Progress of electrospray and electrospinning in energy applications. *Nanotechnology* **2020**, *31*, 132001.

[42] Li, Y.; Zhu, J.; Cheng, H.; Li, G.; Cho, H.; Jiang, M.; Gao, Q.; Zhang, X. Developments of advanced electrospinning techniques: A critical review. *Advanced Materials Technologies* **2021**, *6*, 2100410.

[43] Chuisaca-Londa, E.; Osorio-Ordóñez, D.; Dávalos-Monteiro, J.; Ramirez-Cando, L.; Dávalos-Monteiro, R. CONVERTING POLYMERIC SOLUTIONS INTO BIOMEDICAL NANOFIBERS THROUGH ELECTROSPINNING-AN OVERVIEW OF WORKING PARAMETERS. *Acta Microscopica* **2023**, *32*, pp12–pp29.

[44] Rahma, A.; Munir, M. M.; Prasetyo, A.; Suendo, V.; Rachmawati, H. Intermolecular interactions and the release pattern of electrospun curcumin-polyvinyl (pyrrolidone) fiber. *Biological and Pharmaceutical Bulletin* **2016**, *39*, 163–173.

[45] Lamastra, F. R.; Nanni, F.; Camilli, L.; Matassa, R.; Carbone, M.; Gusmano, G. Morphology and structure of electrospun CoFe2O4/multi-wall carbon nanotubes composite nanofibers. *Chemical Engineering Journal* **2010**, *162*, 430–435.

[46] others,, *et al.* Modification of cellulose acetate nanofibers with PVP/Ag addition. *Materials science in semiconductor processing* **2014**, *28*, 13–19.

[47] Moran, C. H.; Rycenga, M.; Zhang, Q.; Xia, Y. Replacement of poly (vinyl pyrrolidone) by thiols: a systematic study of Ag nanocube functionalization by surface-enhanced Raman scattering. *The Journal of Physical Chemistry C* **2011**, *115*, 21852–21857.

[48] Mina-Villarreal, M. C.; Briceño, S.; Vizuete, K.; Debut, A.; González, G. Growth of carbon nanotubes and carbon spheres on diatoms. *Journal of Porous Materials* **2023**, *30*, 343–349.

[49] Pusporini, P.; Edikresnha, D.; Sriyanti, I.; Suciati, T.; Munir, M. M.; Khairurrijal, K. Electrospun polyvinylpyrrolidone (PVP)/green tea extract composite nanofiber mats and their antioxidant activities. *Materials Research Express* **2018**, *5*, 054001.

[50] Suwanchawalit, C.; Somjit, V. A facile hydrothermal synthesis of magnetic CoFe2O4 nanoparticles and photocatalytic performance. *Dig J Nanomater Bios* **2015**, *10*, 705–713.

[51] Cannas, C.; Musinu, A.; Ardu, A.; Orru, F.; Peddis, D.; Casu, M.; Sanna, R.; Angius, F.; Diaz, G.; Piccaluga, G. CoFe2O4 and CoFe2O4/SiO2 core/shell nanoparticles: magnetic and spectroscopic study. *Chemistry of Materials* **2010**, *22*, 3353–3361.

[52] Briceño, S.; Reinoso, C. CoFe2O4-chitosan-graphene nanocomposite for glyphosate removal. *Environmental Research* **2022**, *212*, 113470.

[53] Bahgat, M.; Farghali, A.; El Rouby, W.; Khedr, M. Synthesis and modification of multi-walled carbon nano-tubes (MWCNTs) for water treatment applications. *Journal of Analytical and Applied Pyrolysis* **2011**, *92*, 307–313.

[54] Mousavi, S. F.; Roein, Z.; Hekmatara, S. H. Multi-walled carbon nanotubes wrapped with polyvinylpyrrolidone can control the leaf yellowing of Alstroemeria cut flowers. *Scientific Reports* **2022**, *12*, 14232.

[55] Lanus Mendez Elizalde, M.; Acha, C.; Molina, F. V.; Antonel, P. S. Composites of poly (3, 4-ethylenedioxythiophene) and CoFe2O4 nanoparticles: composition influence on structural, electrical, and magnetic properties. *The Journal of Physical Chemistry C* **2020**, *124*, 6884–6895.

[56] Alghamdi, H. M.; Rajeh, A. Synthesis of CoFe2O4/MWCNTs nanohybrid and its effect on the optical, thermal, and conductivity of PVA/CMC composite as an application in electrochemical devices. *Journal of Inorganic and Organometallic Polymers and Materials* **2022**, *32*, 1935–1949.

[57] Jauhar, S.; Kaur, J.; Goyal, A.; Singhal, S. Tuning the properties of cobalt ferrite: a road towards diverse applications. *RSC advances* **2016**, *6*, 97694–97719.

[58] others,, *et al.* Electrical and thermal characterization of electrospun PVP nanocomposite fibers. *Journal of Nanomaterials* **2013**, *2013*.